The American Journal of Pathology, Vol. 187, No. 11, November 2017

The American Journal of
PATHOLOGY
ajp.amjpathol.org

VASCULAR BIOLOGY, ATHEROSCLEROSIS, AND ENDOTHELIUM BIOLOGY

Deletion of Endothelial Transforming Growth Factor–β Signaling Leads to Choroidal Neovascularization

Anja Schlecht,* Sarah V. Leimbeck,* Herbert Jägle,† Annette Feuchtinger,‡ Ernst R. Tamm,* and Barbara M. Braunger*

From the Institute of Human Anatomy and Embryology, University of Regensburg, Regensburg; the Department of Ophthalmology,† University Clinic Regensburg, Regensburg; and the Research Unit Analytical Pathology,‡ Helmholtz Zentrum Munich, Munich, Germany*

Accepted for publication
June 29, 2017.

Address correspondence to Barbara M. Braunger, M.D., Ph.D., or Ernst R. Tamm, M.D., Institute of Human Anatomy and Embryology, University of Regensburg, Universitätsstrasse 31, D-93053 Regensburg, Germany. E-mail: barbara.braunger@ur.de or ernst.tamm@ur.de.

The molecular pathogenesis of choroidal neovascularization (CNV), an angiogenic process that critically contributes to vision loss in age-related macular degeneration, is unclear. Herein, we analyzed the role of transforming growth factor (TGF)-β signaling for CNV formation by generating a series of mutant mouse models with induced conditional deletion of TGF-β signaling in the entire eye, the retinal pigment epithelium (RPE), or the vascular endothelium. Deletion of TGF-β signaling in the eye caused CNV, irrespectively if it was ablated in newborn or 3-week–old mice. Areas of CNV showed photoreceptor degeneration, multilayered RPE, basal lamina deposits, and accumulations of monocytes/macrophages. The changes progressed, leading to marked structural and functional alterations of the retina. Although the specific deletion of TGF-β signaling in the RPE caused no obvious changes, specific deletion in vascular endothelial cells caused CNV and a phenotype similar to that observed after the deletion in the entire eye. We conclude that impairment of TGF-β signaling in the vascular endothelium of the eye is sufficient to trigger CNV formation. Our findings highlight the importance of TGF-β signaling as a key player in the development of ocular neovascularization and indicate a fundamental role of TGF-β signaling in the pathogenesis of age-related macular degeneration. *(Am J Pathol 2017, 187: 2570–2589; http://dx.doi.org/10.1016/j.ajpath.2017.06.018)*

The therapeutic options for treating age-related macular degeneration (AMD), the leading cause of vision loss and blindness in industrialized countries,[1–3] are limited.[4,5] AMD is a complex disease[6] whose molecular pathogenesis is not well understood.[4,5] Vision loss in AMD is caused by choroidal neovascularization (CNV) or geographic atrophy.[4,5,7] In geographic atrophy (late dry AMD), the progressive atrophy of the retinal pigment epithelium (RPE) and of the choriocapillaris are likely causes of photoreceptor degeneration.[5] Angiogenic processes that cause immature choroidal vessels to break in and through the RPE into the subretinal space characterize CNV.[8] The resulting blood and plasma leakage causes fibrous scarring of the retina (wet AMD). The pathogenic mechanisms underlying the onset of CNV in AMD are unclear. Dysfunction of the RPE and a dysregulation of proangiogenic and immune-stimulating molecular factors in the region of the retinal/choroidal interface are considered as contributing factors.[4,7,9,10]

The choroidal vasculature forms the choriocapillaris, a vascular bed of highly anastomosed capillaries that is essential for nutrition and oxygen supply of both photoreceptors and RPE.[11] The capillaries have a fenestrated endothelial layer and are highly permeable,[12] a substantial difference from retinal capillaries. There is evidence from several studies of genetically engineered mouse models indicating that RPE-derived vascular endothelial growth factor (VEGF) is essential for choriocapillaris maintenance. VEGF is expressed in high amounts by RPE cells during embryonic development and in adult life.[13] If VEGF expression is compromised, formation of the choriocapillaris in development or its maintenance in adult eyes is severely impaired, leading to choriocapillaris ablation.[14–18]

Supported by German Research Council grants FOR1075 (E.R.T.), TP5 (E.R.T.), and BR 4957/3-1 (B.M.B.).
Disclosures: None declared.

http://dx.doi.org/10.1016/j.ajpath.2017.06.018

Other growth factors that are secreted by RPE cells in high amounts are transforming growth factor (TGF)-β1 and TGF-β2,[19] causing a concentration of both factors in the RPE/choroid complex that is >10-fold higher than in the retina.[20] A recent study showed that a conditional ocular deletion of TGF-β signaling results in pronounced structural changes of retinal capillaries, including the formation of abundant microaneurysms, leaky capillaries, and retinal hemorrhages. Overall, a phenotype resulted similar to that of diabetic retinopathy in humans.[21]

Because TGF-βs are present at high concentrations in the region of the RPE/choroid interface, we wondered if TGF-β signaling might not only be required for stability of retinal capillaries, but also for that of the choriocapillaris. To this end, we targeted the TGF-β type II receptor (TβRII), which is essential for TGF-β signaling, and generated a series of mutant mouse strains with an induced conditional deletion in the entire eye, the RPE, or vascular endothelial cells. Herein, we provide evidence that impairment of TGF-β signaling in the vascular endothelium of the eye is sufficient for the development of CNV. Our findings highlight the importance of the TGF-β signaling pathway as a key player in the development of ocular neovascularization and indicate a fundamental role of TGF-β signaling in the pathogenesis of AMD.

Materials and Methods

Mice

All experiments were performed in mice of either sex that were tested negatively for the *Rd8* mutation.[22] Mice with two floxed alleles of *Tgfbr2* (*Tgfbr2*$^{fl/fl}$)[23] were crossed with heterozygous *CAGGCre-ER*,[24] *VMD2*^{rtTA}*-Cre*,[25] or *VECad-Cre-ER*^{T2}[26] mice. Resulting *Tgfbr2*$^{fl/fl}$*;CAGGCre-ER*, *Tgfbr2*$^{fl/fl}$*;VMD2*^{rtTA}*-Cre*, or *Tgfbr2*$^{fl/fl}$*;VECad-Cre-ER*^{T2} mice were used as experimental mice. For simplicity, *Tgfbr2*$^{fl/fl}$*;CAGGCre-ER* mice will be referred to as *Tgfbr2*$^{\Delta eye}$, *Tgfbr2*$^{fl/fl}$*;VMD2*^{rtTA}*-Cre* mice will be referred to as *Tgfbr2*$^{\Delta RPE}$, and *Tgfbr2*$^{fl/fl}$*;VECad-Cre-ER*^{T2} mice will be referred to as *Tgfbr2*$^{\Delta EC}$. *Tgfbr2*$^{fl/fl}$ littermates with two unrecombined *Tgfbr2* alleles served and are referred to as controls. Genetic backgrounds were 129SV (*Tgfbr2*$^{fl/fl}$, *VMD2*^{rtTA}*-Cre*, and *VECad-Cre-ER*^{T2}) and C57/Bl6 (*CAGGCre-ER*). All mice were reared in a light/dark cycle of 12 hours (lights on at 7 AM). Genotypes were identified by isolating genomic DNA from tail biopsy specimens, and testing for transgenic Cre sequences and floxed *Tgfbr2* sequences, as described previously.[21,27]

Induction of Cre Recombinase

Cre recombinase in *CAGGCre-ER* and *VECad-Cre-ER*^{T2} mice is tamoxifen dependent. In *CAGGCre-ER* mice, the *Cre-ER* fusion protein is ubiquitously expressed. Cre recombinase is restricted to the cytoplasm and will only access the nucleus after binding to tamoxifen.[24,28] *VECad-Cre-ER*^{T2} mice carry the Cre-ER^{T2} expression cassette under regulatory control of the mouse vascular endothelial−cadherin gene promoter region that specifically drives gene expression in the vascular endothelium.[26] To activate Cre recombinase in *Tgfbr2*$^{\Delta eye}$ and*Tgfbr2*$^{\Delta EC}$ mice, the conditional knockout animals and their respective control littermates were equally treated with tamoxifen containing eye drops from postnatal day (P) 4 to P8, as described previously.[29] A second stock of *Tgfbr2*$^{\Delta eye}$ and control mice was treated from P21 to P25, a time when the development of the retinal vasculature is complete. For simplicity, *Tgfbr2*$^{\Delta eye}$ mice that were tamoxifen treated from P4 to P8 will be referred to as early induced, and *Tgfbr2*$^{\Delta eye}$ mice that were tamoxifen treated from P21 to P25 will be referred to as late induced. Cre recombinase in *VMD2*^{rtTA}*-Cre*;*Tgfbr2*$^{fl/fl}$ is doxycycline dependent and under the control of the RPE-specific bestrophin promotor.[25] Doxycycline (AppliChem, Darmstadt, Germany) was diluted in phosphate-buffered saline (PBS) to a final concentration of 0.1 g/mL, and doxycycline eye drops (10 μL) were pipetted onto the eyes of *Tgfbr2*$^{\Delta RPE}$ mice and their control littermates from P21 to P25 three times per day. A detailed list of the individual treatment time points and subsequently performed analyses of the eyes is presented in Table 1.

mT/mG and *R26R* Reporter Mice

The efficiency of the Cre recombinase activation in *VeCad-Cre-ER*^{T2} mice was confirmed using *mT/mG* reporter mice,[30] which express a membrane-targeted green fluorescent protein after Cre-mediated excision. Heterozygous *VeCad Cre-ER*^{T2} mice were crossed with homozygous *mT/mG* mice. The resulting offspring (*VeCad-Cre-ER*$^{T2+/-}$*;mT/mG*$^{+/-}$ and *wildtype;mT/mG*$^{+/-}$) were treated with tamoxifen eye drops from P4 to P8, according to previously published protocols.[21,29] Mice were euthanized at P10. After enucleation, the eyes were fixed in 4% paraformaldehyde (PFA) for 4 hours, washed extensively in phosphate buffer (PB; 0.1 mol/L, pH 7.4), incubated in 10%, 20%, and 30% sucrose overnight, and shock frozen in tissue-mounting medium (O.C.T. Compound; DiaTec, Bamberg, Germany). Frozen sections were washed three times in PB (5 minutes each), and cell nuclei were counterstained with DAPI (Vectashield; Vector Laboratories, Burlington, CA) 1:10 diluted in fluorescent mounting medium (Serva, Heidelberg, Germany). Successful activation of the Cre recombinase in *CAGG-Cre-ER* mice was confirmed using Rosa26 reporter (*R26R*) reporter mice.[31] Heterozygous *CAGGCre-ER* mice were crossed with homozygous *R26R* mice. The resulting offspring were treated with tamoxifen eye drops from P21 to P25, according to previously published protocols.[27,29] Mice were euthanized at the age of 4 weeks, and the eyes were enucleated and processed for LacZ staining, which was performed as described previously.[29,32]

Table 1 Treatment Time Points and Performed Analyses

Mouse model	Treatment	Performed analyses	Age
Tgfbr2$^{\Delta eye}$ and controls	Tamoxifen P4-P8	Morphology	2 and 3 months
		FITC-dextran	6 weeks
		3D imaging	6 weeks
		Electron microscopy	2.5 months
		RNA analyses	6 weeks
		Immunohistochemistry	4 and 6 weeks
Tgfbr2$^{\Delta eye}$ and controls	Tamoxifen P21-P25	Morphology	3 and 6 months
		FITC-dextran	2 months
		Angiography	3 and 6 months
		ERG	3 and 6 months
		Electron microscopy	3 months
		RNA analyses	5 weeks
		Immunohistochemistry	3 months
Tgfbr2$^{\Delta EC}$ and controls	Tamoxifen P4-P8	Morphology	6 weeks
		FITC-dextran	6 weeks
		Electron microscopy	4 and 6 weeks
		Immunohistochemistry	4 and 6 weeks
Tgfbr2$^{\Delta RPE}$ and controls	Doxycyclin P21-P25	Morphology	6 months
		Angiography	6 months

3D, three dimensional; ERG, electroretinography; FITC, fluorescein isothiocyanate; P, postnatal day.

Paraffin sections were analyzed by light microscopy (Carl Zeiss, Jena, Germany).

Tgfbr2 Deletion PCR

Tgfbr2 deletion PCR screens its successful genomic deletion after Cre-mediated recombination. DNA samples of the sensory retina and the choroid (including cells of the RPE) served as templates. Primer pairs and protocols are described elsewhere.[29,33] Actin was used as the loading control.

Morphology and Microscopy

Eyes were enucleated, fixed for 24 hours in 2% PFA/2.5% glutaraldehyde,[34] and embedded in Epon (Serva), as described elsewhere.[35,36] Semithin meridional sections (1 μm thick) were cut through the eyes and stained, according to the method of Richardson et al.[37] The sections were analyzed on an Axio Imager Z1 microscope (Carl Zeiss) using Axiovision software version 4.8 (Carl Zeiss). Ultrathin sections were processed according to protocols published previously,[38,39] stained with uranyl acetate and lead citrate, and analyzed on a transmission electron microscope (Libra; Carl Zeiss).

Immunohistochemistry

Before TβRII, collagen IV, and VEGF-A staining, eyes were fixed for 4 hours in 4% PFA, washed extensively in PB (0.1 mol/L, pH 7.4), and embedded in paraffin, according to standard protocols. Paraffin sections (6 μm thick) were deparaffinized and washed in water. For detection of TβRII, sections were treated with boiling citrate buffer (1 × 10 minutes, pH 6), washed again in water, and incubated in PB. For detection of collagen IV and VEGF-A, sections were pretreated with 0.05 mol/L Tris-HCl (5 minutes) and covered with Proteinase K [100 μL of Proteinase K in 57 mL of Tris-HCl (0.05 mol/L), 5 minutes], washed in water, incubated in 2N HCl (20 minutes), and washed again in water. Sections were incubated in PB for 5 minutes and then blocked with 2% bovine serum albumin, 0.2% cold water fish gelatine, and 0.1% Triton X (TβRII), 2% bovine serum albumin and 0.1% Triton X (collagen IV), or 5% nonfat dry milk (VEGF-A) at room temperature for 60 minutes. Primary antibodies (Table 2) were diluted in a 1:10 dilution of blocking solution in PB. Before F4/80 and plasmalemma vesicle-associated protein (PLVAP) staining, eyes were fixed for 4 hours in 4% PFA, washed extensively in PB, incubated in 10%, 20%, and 30% sucrose/PBS overnight at 4°C, and shock frozen in tissue-mounting medium. For immunohistochemistry, frozen sections were washed three times in PB or PBS (F4/80) for 5 minutes each and blocked at room temperature with 2% bovine serum albumin in PB for 45 minutes (F4/80: 1% nonfat dry milk and 0.01% Tween in PB). Primary antibodies (Table 2) were diluted in a 1:10 dilution of blocking solution in PB (F4/80: 2% bovine serum albumin, 0.02% NaN_3, and 0.01% Triton X in PBS), and incubated at 4°C overnight. After three washes in PB/PBS (5 minutes each), biotinylated antibodies were applied for 1 hour and diluted in a 1:10 dilution of the blocking solution. Then, appropriate secondary antibodies (Table 2), diluted in a 1:10 dilution of the blocking solution, were applied on the sections for 1 hour. Sections were washed again three times in PB/PBS, and cell nuclei were counterstained with DAPI (Vectashield) diluted (1:10) in

Table 2 Antibodies Used for Immunohistochemistry

Primary antibody (manufacturer)	Secondary antibody (manufacturer)
TβRII-L21 (Santa Cruz Biotechnology, Dallas, TX), 1:20	Anti-rabbit, biotinylated (Vector Laboratories, Burlington, CA), 1:500; streptavidin Alexa 488 (Invitrogen, Carlsbad, CA), 1:1000
Collagen IV (Rockland Immunochemicals Inc., Limerick, PA), 1:100	Anti-rabbit Cy-3 conjugated (Jackson Immuno Research Labs, West Grove, PA), 1:2000
VEGF-A (R&D Systems, Minneapolis, MN), 1:50	Anti-goat, biotinylated (Vector Laboratories), 1:500; streptavidin Alexa 546 (Invitrogen), 1:1000
F4/80 (Acris Antibodies GmBH, Herford, Germany), 1:600	Anti-rat Cy-3 conjugated (Jackson Immuno Research Labs), 1:2000, in PBS
PLVAP (Santa Cruz Biotechnology), 1:50	Anti-rat Cy-3 conjugated (Jackson Immuno Research Labs), 1:2000

In all cases, fixation was performed with 4% paraformaldehyde.

PBS, phosphate-buffered saline; PLVAP, plasmalemma vesicle-associated protein; TβRII, transforming growth factor-β type II receptor.

fluorescent mounting medium (Serva). Sections were investigated on an Axio Imager Z1 fluorescent microscope using appropriate Axiovision software.

Quantification of F4/80-Positive Cells on Immunohistochemical Sections

Experimenters (A.S. and B.M.B.) were blinded regarding the genotype. Antibody incubation times were strictly monitored, and microscope settings (eg, the illumination time and intensity) were identical between individual sections. Only sections in midsagittal orientation were analyzed that stretched through the optic nerve to ensure comparable situations between the individual sections. F4/80-positive cells were counted per hemisphere in the retina and in the choroid/choriocapillaris.

Dextran Perfusion

Before dextran perfusion, mice were deeply anesthetized with ketamine [120 mg/kg body weight (bw)] and xylazine (8 mg/kg bw). Afterward, mice were perfused through the left ventricle with 1 mL of PBS containing 50 mg fluorescein isothiocyanate (FITC)—dextran (mol. wt., 2000 kDa; TdB Consultancy, Uppsala, Sweden). The eyes were enucleated and fixed in 4% PFA for 2 hours (flat mounts)/4 hours (sections) and washed in PB. Eyes were cut into sections, placed on glass slides, and counterstained with DAPI (Vectashield) 1:10 diluted in fluorescent mounting medium. FITC-dextran perfused sections were investigated on an Axio Imager Z1 fluorescent microscope.

Quantification of CNV

After dextran perfusion, flat mounts of the posterior eye segment (containing the retina, RPE, choroid, and sclera) were dissected. Similar to the preparation of retinal flat mounts, the posterior eye segment was flat mounted on glass slides using fluorescent mounting medium. The entire flat mount was analyzed using an Axio Imager Z1 fluorescent microscope. Focusing on the retinal pigment epithelium allowed the quantification of the CNV penetrating through the RPE. To visualize the CNV, Z-stacks were generated that ranged from the superficial retinal plexus to the optical barrier of the pigmented RPE.

ERG Data

Mice were dark adapted for at least 12 hours before the experiments and anesthetized by s.c. injection of ketamine (65 mg/kg bw) and xylazine (13 mg/kg bw). Pupils were dilated with tropicamide eye drops (Mydriaticum Stulln; Pharma Stulln GmbH, Stulln, Germany). Silver needle electrodes served as reference (forehead) and ground (tail), and gold wire ring electrodes served as active electrodes. Electroretinograms (ERGs) were recorded with a Ganzfeld bowl (Ganzfeld QC450 SCX; Roland Consult, Brandenburg, Germany) and an amplifier/recording unit (RETIPort; Roland Consult), band pass filtered (1 to 300 Hz), and averaged. Single-flash scotopic (dark-adapted) responses to a series of 10 light-emitting diode flash intensities (range, −3.5 to 1.0 log cd · second/m^2) were recorded. After 10 minutes of adaption to a white background illumination (20 cd/m^2), single-flash photopic (light-adapted) responses to three xenon-flash intensities (1, 1.5, and 2 log cd · second/m^2) were recorded. All analyses and plotting were performed with R version 3.2.1 (The R Foundation for Statistical Computing, Vienna, Austria) and ggplot2 version 2.1.0.[40]

Fundus Imaging and Angiography

Imaging of the retinal vasculature was performed with a commercially available imaging system (Micron III; Phoenix Research Laboratories, Pleasanton, CA). Light source and imaging path filters (low and high pass at 500 nm) were used for fluorescein angiography. Mice were anesthetized by s.c. injection of ketamine (65 mg/kg bw) and xylazine (13 mg/kg bw), and their pupils were dilated with tropicamide eye drops before image acquisition. Fluorescein angiography was performed with s.c. injection of 75 mg/kg bw fluorescein-sodium (Alcon, Hünenberg, Switzerland).

Table 3 Primers Used for Real-Time PCR Amplification

Gene	Sequence forward	Sequence reverse
GAPDH	5′-TGTCCGTCGTGGATCTGAC-3′	5′-CCTGCTTCACCACCTTCTTG-3′
GNB2L	5′-TCTGCAAGTACACGGTCCAG-3′	5′-ACGATGATAGGGTTGCTGCT-3′
RPL32	5′-GCTGCCATCTGTTTTACGG-3′	5′-TGACTGGTGCCTGATGAACT-3′
Tgfbr2	5′-AGAAGCCGCATGAAGTCTG-3′	5′-GGCAAACCGTCTCCAGAGTA-3′
Ccl2	5′-CATCCACGTGTTGGCTCA-3′	5′-GATCATCTTGCTGGTGAATGAGT-3′
Cd68	5′-CTCTCTAAGGCTACAGGCTGCT-3′	5′-TCACGGTTGCAAGAGAAACA-3′
Gfap	5′-TCGAGATCGCCACCTACAG-3′	5′-GTCTGTACAGGAATGGTGATGC-3′
Il-6	5′-GCTACCAAACTGGATATAATCAGGA-3′	5′-CCAGGTAGCTATGGTACTCCAGAA-3′
iNos	5′-GGGCTGTCACGGAGATCA-3′	5′-CCATGATGGTCACATTCTGC-3′
Tnf-α	5′-TCTTCTCATTCCTGCTTGTGG-3′	5′-GGTCTGGGCCATAGAACTGA-3′
Vegf-a-120	5′-AAAGCCAGCACATAGGAGAG-3′	5′-GGCTTGTCACATTTTTCTGG-3′
Vegf-a-164	5′-GAACAAAGCCAGAAAATCACTGTG-3′	5′-CGAGTCTGTGTTTTTGCAGGAAC-3′
Fgf2	5′-CGGCTCTACTGCAAGAACG-3′	5′-TGCTTGGAGTTGTAGTTTGACG-3′

RNA Analysis

Total RNA from retinas was extracted with TriFast (Peqlab Biotechnologie GmbH, Erlangen, Germany), and first-strand cDNA synthesis was performed with the iScript cDNA Synthesis Kit (Bio-Rad Laboratories, Inc., Hercules, CA), according to the manufacturer's guidelines. Real-time quantitative RT-PCR analyses were performed with the iQ5 Realtime PCR Detection System (Bio-Rad Laboratories, Inc.). The temperature profile was denaturation at 95°C for 10 seconds and annealing and extension at 60°C for 40 seconds for 40 cycles. All primer pairs were purchased from Invitrogen (Carlsbad, CA) and extended over exon-intron boundaries, except for *Gapdh*. Sequences of primer pairs are shown in Table 3. RNA that was not reverse transcribed served as a negative control for real-time RT-PCR. Before relative quantification, mRNAs from three different potential housekeeping genes were tested: glyceraldehyde 3-phosphate dehydrogenase, guanine nucleotide binding protein, and ribosomal protein L32. Statistical analyses were performed to confirm that none of the housekeeping genes were regulated and then the geometric mean of the crossing thresholds of all three housekeeping genes was used for relative quantification. Quantification was performed using BioRad iQ5 Standard-Edition software version 2.1 (Bio-Rad Laboratories GmbH, Munich, Germany) and the ΔΔCt method in Excel (Microsoft Corp., Redmond, WA).[41]

Deep Tissue Imaging by Three-Dimensional Light-Sheet Fluorescence Microscopy

Mice were deeply anesthetized with ketamine (120 mg/kg bw) and xylazine (8 mg/kg bw), and 130 μL of *Tomato lectin* (Perkin Elmer, Inc., Waltham, MA) was slowly injected intravenously. Mice were euthanized 15 minutes after injection by cervical dislocation. The eyes were enucleated and fixed using Paxgene Tissue Containers (Qiagen, Hilden, Germany), according to the manufacturer's recommendations, and thereafter underwent a chemical procedure of optical clearing, as previously described.[42] Cleared transparent whole mouse eyes were imaged on a light-sheet fluorescence microscope (UltraMicroscope II; LaVision BioTec, Bielefeld, Germany), equipped with an sCMOS camera (Andor Neo, Concord, MA) and a 2×/0.5 numerical aperture objective lens (MVPLAPO 2×; Olympus, Hamburg, Germany). The specimens were two sided, illuminated by a planar light sheet using a white light laser (SuperK EXTREME EXW-9; NKT Photonics, Birkeröd, Denmark). To visualize the specific TLectinSense 680 signals for vascularization, a bandpass filter set with an excitation range of 640/30 nm and an emission range of 690/50 nm was used in combination with an additional filter set (excitation, 531/40 nm; emission, 593/40 nm) for detection of autofluorescence (morphology). By moving the specimen chamber vertically stepwise (step size, 4 μm) through the laser light sheet, optical sections were obtained. To ensure standardized imaging regions for each eye, the scan always covered 600 μm above to 600 μm below the optical nerve. Maximum intensity projections were performed by ImspectorPro software version 5.0 (LaVision BioTec, Bielefeld, Germany).

Statistical Analysis

All results are expressed as means ± SEM. Comparisons between the mean variables of two groups were made by a two-tailed *t*-test. Significance of the ERG analyses was evaluated using a one-way analysis of variance test, followed by a Tukey honest significant difference post hoc test. $P \leq 0.05$ was considered statistically significant.

Study Approval

All procedures conformed to the tenets of the NIH's *Guide for the Care and Use of Laboratory Animals*,[43] European Union Directive 2010/63/E, and institutional guidelines;

all procedures were approved by the local authority (Regierung der Oberpfalz, AZ 54-2532.1-44/12 and DMS 2532-2-85).

Results

Deletion of Ocular TGF-β Signaling in Mouse Pups Leads to Choroidal Neovascularization

To investigate the role of the TGF-β signaling pathway for the structure of retinal and choroidal vessels, the essential TβRII receptor in the eyes was removed via tamoxifen-induced conditional deletion. To this end, *Tgfbr2fl/fl;CAGGCre-ER* mice were generated and treated from P4 to P8 with tamoxifen eye drops. For simplicity, *Tgfbr2fl/fl;CAGGCre-ER* mice that received tamoxifen by this protocol will be referred to as early-induced $Tgfbr2^{\Delta eye}$ mice, and tamoxifen-treated littermates with two unrecombined $Tgfbr2^{fl/fl}$ alleles are referred to as controls. As shown previously, the treatment results in a significant reduction of TβRII and its mRNA in the eyes of early-induced $Tgfbr2^{\Delta eye}$ mice compared to controls.[21] The previous study also showed that the deletion of ocular TGF-β signaling leads to the formation of abundant microaneurysms in retinal vessels and to a phenotype that largely mimics that of non-proliferative and proliferative diabetic retinopathy in humans.[21] Consequently, the retina of 2- and 3-month−old early-induced $Tgfbr2^{\Delta eye}$ mice contained vascular microaneurysms in the inner nuclear layer, which were characterized by their large lumen and thick coat of endothelial cells (Figure 1, A−C). In contrast, no changes were seen in control mice (Figure 1, A and B). We now turned our attention to the choroidal/retinal interface that had not been analyzed previously. Herein, we frequently observed focal areas in which the outer segments of photoreceptors were completely missing and the thickness of the outer nuclear layer was substantially reduced (Figure 1, B and C). Accumulations of cells were present between photoreceptors and RPE. The cells frequently surrounded vascular openings filled with erythrocytes, strongly indicating their endothelial origin and an ongoing neoangiogenetic process. The RPE was multilayered in those areas, and contained cystic and amorphous inclusions (Figure 1C). When investigating serial sections, we observed vessels beneath and above the RPE, concomitant with type 1 (sub-RPE, occult) and type 2 (subretinal, classic) CNV in human patients.

To characterize the origin of the newly formed vessels in the subretinal space (between the sensory retina and the RPE) of early-induced $Tgfbr2^{\Delta eye}$ mice, we perfused the mice with high-mol. wt. FITC-dextran for vascular labeling. Although the retinal and choroidal vasculature of control animals was essentially normal, distinct changes were observed in the subretinal space of early-induced $Tgfbr2^{\Delta eye}$ mice. Vessels were observed breaking from the choroid through the Bruch membrane (BM) across the RPE into the subretinal space (Figure 2A). FITC-dextran−perfused flat-mounted posterior eye segments (containing the retina, RPE, choroid, and sclera) of 4- to 6-week−old animals had 2.86 ± 0.59 CNVs per eye ($n = 7$) (Supplemental Figure S1B). To confirm this observation by an independent method, three-dimensional imaging of lectin-perfused, optical-cleared, and transparent whole eyes was performed (Figure 2B). The choriocapillaris did not resolve into single capillaries but rather appeared as an intense fluorescent line covering the outer surface of the retina, a fact attributed to the immense density and blood flow of this capillary bed.[44] In control eyes, the three plexuses of the retinal vasculature could be completely visualized and were essentially normal. In contrast, in early-induced $Tgfbr2^{\Delta eye}$ mice, vessels that originated from the choriocapillaris entered the retina and continued into the retinal vascular bed, forming obvious anastomoses with retinal vessels (Figure 2B). We now characterized the vascular wall of the newly formed vessels by transmission electron microscopy. As expected, in control mice, the endothelium surrounding retinal vessels was continuous (Figure 2C), whereas that around the choriocapillaris was fenestrated. When the newly formed vessels in the subretinal space of early-induced $Tgfbr2^{\Delta eye}$ mice were analyzed, distinct fenestrations covered by a typical diaphragm were regularly observed (Figure 2C). To further support this finding, immunohistochemical staining was performed for PLVAP, a vascular protein, an intrinsic component of the diaphragm of vascular fenestrae, and a marker for fenestrated endothelia.[45−48] As expected, in control and early-induced $Tgfbr2^{\Delta eye}$ animals, the continuous endothelium of the retinal vasculature did not show any PLVAP immunoreactivity (Supplemental Figure S1A), whereas the fenestrated endothelium of the choriocapillaris showed an intense PLVAP signal (Figure 2D). In early-induced $Tgfbr2^{\Delta eye}$ mice, intense PLVAP immunoreactivity was observed in the areas of neovascularization in the subretinal space (Figure 2D). Overall, our results strongly indicated that loss of TGF-β signaling in early-induced $Tgfbr2^{\Delta eye}$ mice caused CNV.

TGF-β Signaling Is Required to Prevent CNV in Late-Induced $Tgfbr2^{\Delta eye}$ Mice

Next, we wondered whether the formation of CNV after TβRII deletion might be supported by the facts that retinal vascular development is not completed in mouse pups and that signaling processes that promote angiogenesis are continuously ongoing. To learn if TGF-β signaling is also important for maintenance of the adult choriocapillaris when retinal vascular development is completed, we deleted TGF-β signaling by an essentially comparable approach in 3-week−old mice with completely developed retinal vasculature. Mice were treated with tamoxifen eye drops from P21 to P25 and are further referred to as late-induced $Tgfbr2^{\Delta eye}$ mice. To confirm successful tamoxifen-induced recombination, we crossed the mice with Cre reporter mice carrying the *R26R* allele. Tamoxifen-treated eyes were stained for β-galactosidase, and an intense staining was seen

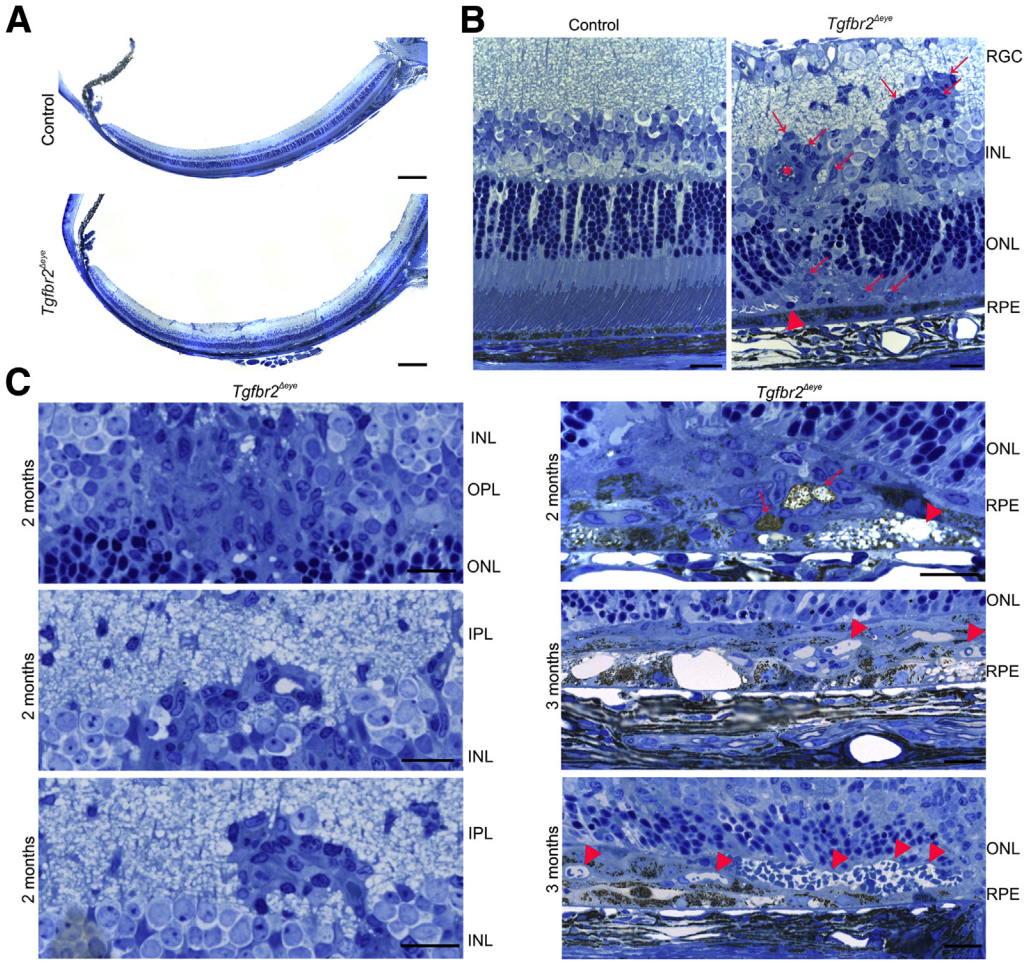

Figure 1 Early-induced deletion of transforming growth factor—β (TGF-β) signaling in the eye causes structural changes in the subretinal space. Stained semithin sections (1 μm thick) of an early-induced *Tgfbr2*$^{\Delta eye}$ mouse and its control littermate, according to the method of Richardson et al.[37] **A:** Retinal hemispheres of 2-month—old control and *Tgfbr2*$^{\Delta eye}$ animals. **B:** Detailed magnification of the retina. The control mouse shows regular structure. In the retina of the *Tgfbr2*$^{\Delta eye}$ mouse, a vessel (**asterisk**) filled with erythrocytes is seen, which disrupts the inner nuclear layer (INL) and outer nuclear layer (ONL) and is surrounded by an accumulation of cells that continue into the subretinal space (**arrows**). In the subretinal space, mononuclear cells (**arrowhead**) are present, whereas photoreceptor outer segments are degenerated and the choroid is thickened. **C, left panels:** In the inner retina of 2-month—old *Tgfbr2*$^{\Delta eye}$ mice, accumulations of endothelial cells are seen in both the ONL/outer plexiform layer (OPL) and in the INL/inner plexiform layer (IPL). **C, right panels:** At the retinal/choroidal interface of 2- and 3-month—old *Tgfbr2*$^{\Delta eye}$ mice, the retinal pigment epithelium (RPE) is multilayered (**arrows** in **top panel**) and contains cystic and amorphous inclusions (**arrowhead** in **top panel**). At the age of 3 months, erythrocyte-containing vessels fill the subretinal space (**arrowheads** in **middle** and **bottom panels**). Scale bars: 200 μm (**A**); 20 μm (**B** and **C**). RGC, retinal ganglion cell.

throughout the eye of *CAGGCre-ER;R26R* mice, whereas ocular tissues of *R26R* littermates, which did not carry the *CAGGCre-ER* transgene, were completely unstained (Supplemental Figure S2A). Furthermore, the significant deletion of retinal *Tgfbr2* was confirmed by real-time RT-PCR analyses (Supplemental Figure S2B). Next, we analyzed the ocular morphology of late-induced *Tgfbr2*$^{\Delta eye}$ mice and controls at the age of 3 (Figure 3, A and B) and 6 (Figure 4, A and C) months. Retinal structure was essentially normal in control animals (Figure 3, A and B, and Figure 4, A and C), and no obvious changes were observed in the inner retina of 3-month—old late-induced *Tgfbr2*$^{\Delta eye}$ animals (Figure 3B). However, similar to our observations in early-induced *Tgfbr2*$^{\Delta eye}$ animals, all of the late-induced *Tgfbr2*$^{\Delta eye}$ mice showed structural changes in the subretinal space that were essentially comparable to that observed in early-induced *Tgfbr2*$^{\Delta eye}$ mice (Figure 3, A and D, and Figure 4, A—C). In focal areas in which photoreceptor outer segments were shortened or completely missing, vessels were observed in the subretinal space. By transmission electron microscopy, a fenestrated endothelial layer was identified surrounding the vessels (Figure 5B). The RPE in those areas was multilayered and frequently contained cystic and amorphous inclusions. In 6-month—old late-induced *Tgfbr2*$^{\Delta eye}$ mice, the choroid was thickened and photoreceptor outer segments were completely missing (Figure 4, A—C). The RPE was reduced to a flat layer or formed focal accumulations in those areas in which subretinal vessels

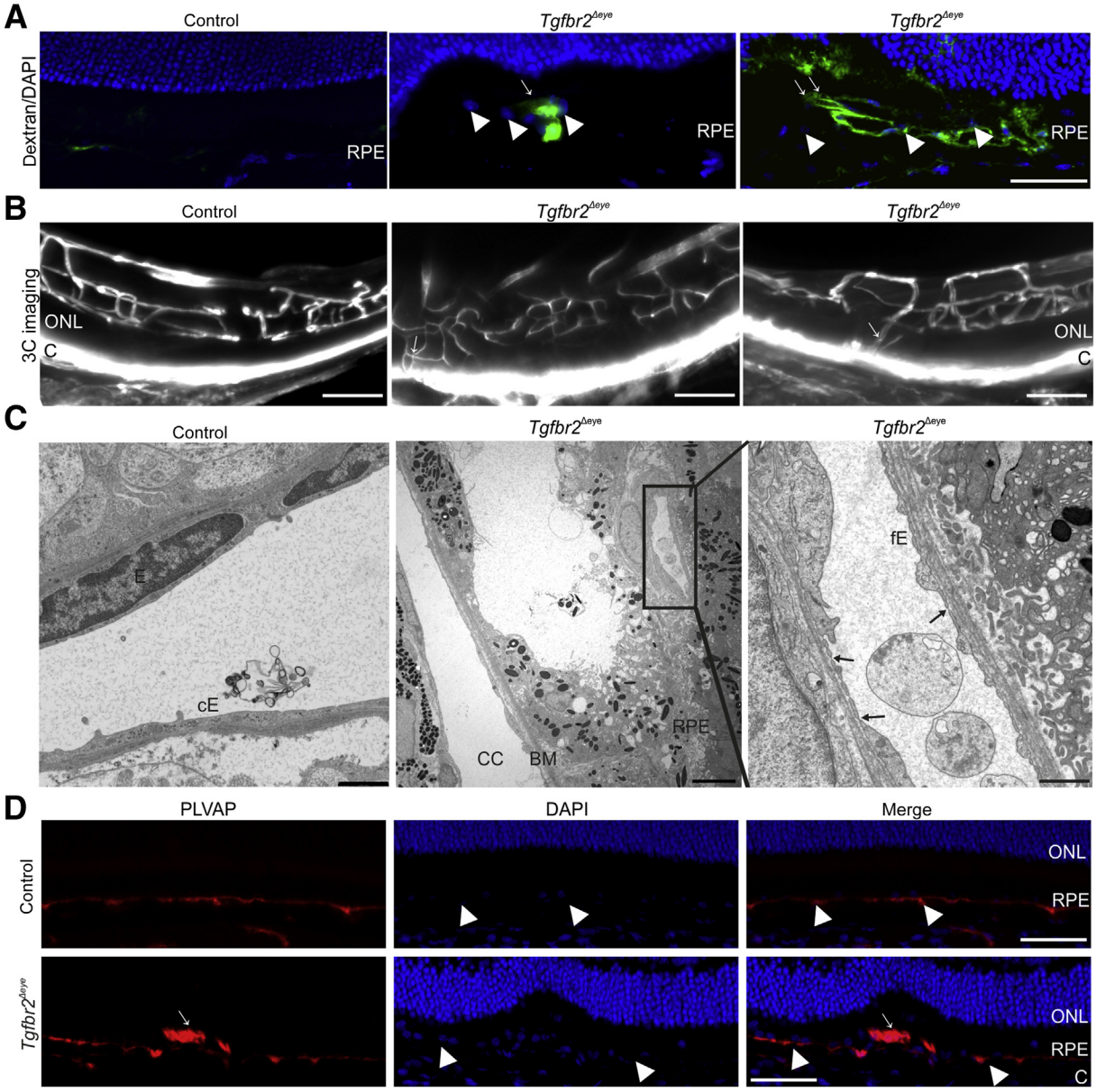

Figure 2 Subretinal neovascularization with fenestrated endothelium (fE) after deletion of transforming growth factor−β (TGF-β) signaling in the eyes of early-induced *Tgfbr2*$^{\Delta eye}$ mice. **A:** Fluorescein isothiocyanate−dextran (green)−perfused retinal meridional section of a control and *Tgfbr2*$^{\Delta eye}$ mouse at 6 weeks of age. **White arrows** point toward choroidal vessels breaking through the Bruch membrane (BM) and retinal pigment epithelium (RPE; nuclei of the RPE marked by **white arrowheads**) into the subretinal space. Nuclei are DAPI stained (blue). **B:** Light-sheet fluorescence microscopy of transparent eyes of 6-week-old lectin-injected *Tgfbr2*$^{\Delta eye}$ mice and a control littermate. The control mouse shows an essentially regular arborized retinal vasculature. The *Tgfbr2*$^{\Delta eye}$ mice have an irregular arrangement of the retinal plexus and form anastomoses between retinal and choroidal vessels (**arrows**). **C:** Transmission electron microscopy of an intraretinal vessel outlined with a continuous endothelium (cE) in a 2.5-month−old control animal. In contrast, the subretinal neovasculature in the *Tgfbr2*$^{\Delta eye}$ littermate has a fE (**black arrows**, **right panel**). The **right panel** shows the **boxed region** of the **middle panel** in higher magnification. **D:** Immunoreactivity for plasmalemma vesicle-associated protein (PLVAP; red) in the retina at 4 weeks of age. The control and the *Tgfbr2*$^{\Delta eye}$ animal show a thin, one-layered PLVAP signal in the choriocapillaris (CC; **white arrowheads**). In addition, the *Tgfbr2*$^{\Delta eye}$ mouse displays PLVAP-positive signals (**white arrows**) in the RPE and subretinal space. Nuclei are DAPI stained (blue). Scale bars: 50 μm (**A** and **D**); 120 μm (**B**); 1000 nm (**C**, **left** and **right panels**); 5000 nm (**C**, **middle panel**). 3D, three dimensional; C, choroid; ONL, outer nuclear layer.

were present. *In vivo* imaging and fluorescein *in vivo* angiography of 3-month−old animals showed a regular fundus and retinal vasculature in both control and late-induced *Tgfbr2*$^{\Delta eye}$ mice (Figure 3C). To investigate the retinal vasculature in more detail, we additionally perfused 2-month−old, late-induced *Tgfbr2*$^{\Delta eye}$ mice with high-mol. wt. FITC-dextran and analyzed the vasculature on meridional sections. The retinal vasculature had a regular

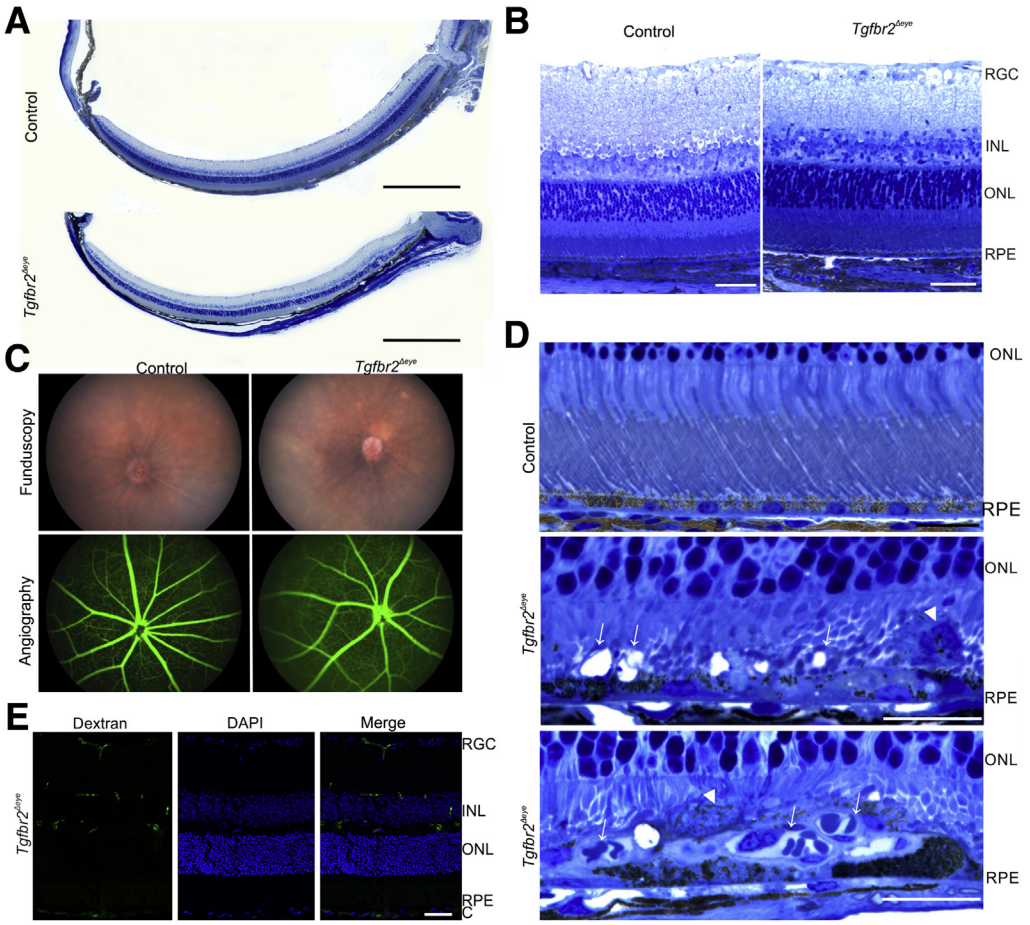

Figure 3 Subretinal neovascularization after deletion of transforming growth factor—β (TGF-β) signaling in the eyes of 3-month—old late-induced *Tgfbr2*$^{\Delta eye}$ mice. **A:** Stained semithin sections (1 μm thick) of the retinal hemispheres of a 3-month—old, late-induced *Tgfbr2*$^{\Delta eye}$ mouse and its control littermate, according to the method of Richardson et al.[37] **B:** Higher magnification of the retinal sections. **C:** *In vivo* funduscopy and fluorescein angiography of a 3-month—old, late-induced *Tgfbr2*$^{\Delta eye}$ mouse and its control littermate. The retinal vasculature and the fundus appear essentially normal. Diameters of the image sections refer to 2 mm retina. **D:** Detailed magnification of stained semithin sections, according to the method of Richardson et al,[37] of the retinal/choroidal interface of 3-month—old *Tgfbr2*$^{\Delta eye}$ mice and a control littermate. The control mouse shows regular structure. *Tgfbr2*$^{\Delta eye}$ mice show focal areas in which the photoreceptor outer segments are shortened or completely missing, with vessels in the subretinal space. In these regions, the retinal pigment epithelium (RPE) is multilayered (**white arrowhead**, **middle** and **bottom panels**) and frequently contains cystic and amorphous inclusions (**white arrows**, **middle panel**). Mononuclear cells (**white arrowhead**, **middle panel**) are visible in the subretinal space. **E:** Fluorescein isothiocyanate—dextran (green)—perfused retinal meridional section of a 2-month—old *Tgfbr2*$^{\Delta eye}$ mouse. The three retinal vascular plexuses are present in their correct localization. Nuclei are DAPI stained (blue). Scale bars: 500 μm (**A**); 50 μm (**B** and **E**); 20 μm (**D**). C, choroid; INL, inner nuclear layer; ONL, outer nuclear layer; RGC, retinal ganglion cell.

appearance, and the vessels were in their anatomically correct localization. Furthermore, we did not observe FITC-dextran or fluorescein leaking into the vitreous, the subretinal space, or the surrounding tissue (Figure 3, C and E). As we had observed a significant reduction of the pericyte marker neural/glial antigen 2 in the retina of early-induced *Tgfbr2*$^{\Delta eye}$ animals,[21] we now focused on the coating of the choroidal vessels with neural/glial antigen 2—positive pericytes in 4-week—old early-induced and 6-week—old late-induced *Tgfbr2*$^{\Delta eye}$ animals. We did not observe a difference in pericyte coverage compared to controls (data not shown). When the eyes at the age of 6 months were analyzed by *in vivo* fundus imaging and fluorescein angiography, control mice showed no pathological changes, in neither the fundus nor the retinal vasculature (Figure 4D). In contrast, in late-induced *Tgfbr2*$^{\Delta eye}$ mice, the fundus was hyperpigmented, indicating RPE proliferation or dedifferentiation; in some animals, the retina had detached (Figure 4D). In parallel to the structural changes, marked functional changes by ERG that reflected the observed gradual degeneration of the retina from 3 to 6 months of age in late-induced *Tgfbr2*$^{\Delta eye}$ mice were detected (Supplemental Figure S3, A—G). Although, in 3-month—old *Tgfbr2*$^{\Delta eye}$ mice, the scotopic responses showed a similar waveform but slightly lower amplitudes compared to control mice, the photopic waveform was unchanged in amplitude and implicit time. However, the difference was not statistically significant. In 6-month—old *Tgfbr2*$^{\Delta eye}$ mice, both the scotopic and photopic responses could not be distinguished from noise in almost all eyes.

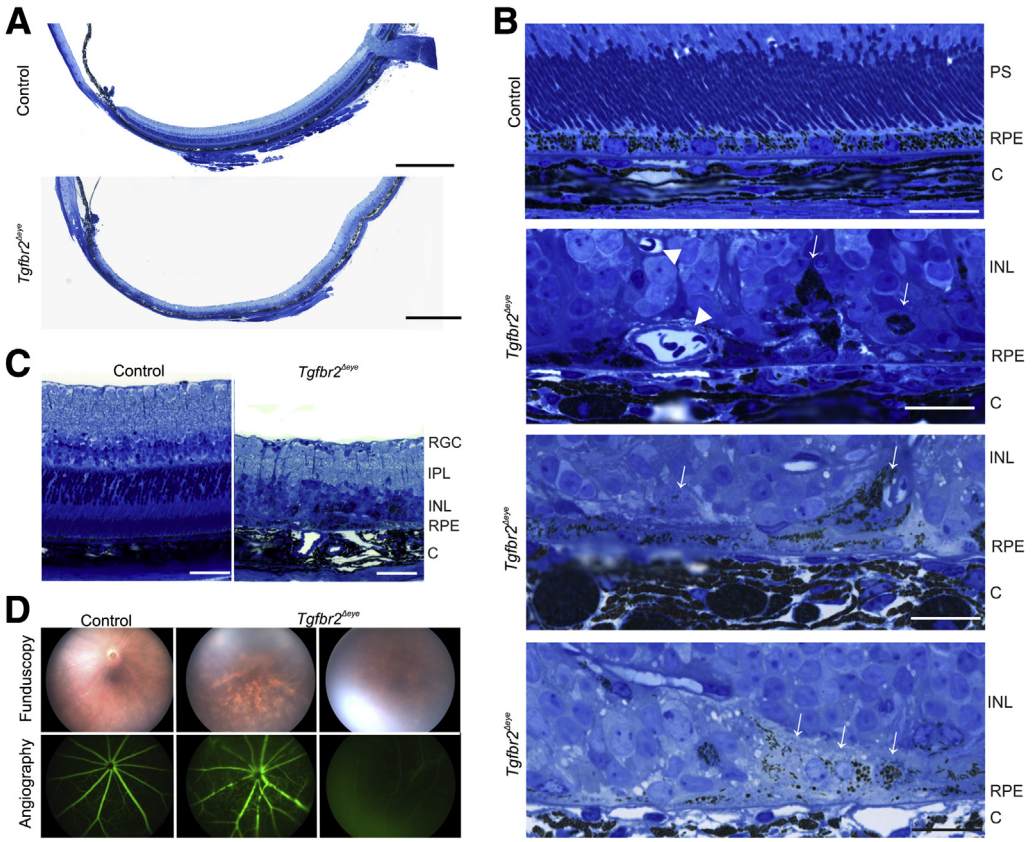

Figure 4 Subretinal neovascularization and retinal degeneration after deletion of transforming growth factor—β (TGF-β) signaling in the eyes of 6-month—old late-induced *Tgfbr2*$^{\Delta eye}$ mice. **A:** Stained semithin sections (1 μm thick) of the retinal hemispheres of 6-month—old animals, according to the method of Richardson et al.[37] The control animal shows regular retinal morphology. In contrast, in the *Tgfbr2*$^{\Delta eye}$ littermate, photoreceptor outer segments are completely degenerated. **B:** Detailed magnification of stained semithin sections of the outer retina and the choroid (C) of 6-month—old *Tgfbr2*$^{\Delta eye}$ mice and a control littermate, according to the method of Richardson et al.[37] The morphology of the control mouse is normal. In contrast, the *Tgfbr2*$^{\Delta eye}$ mouse has erythrocyte-filled vessels in the retinal pigment epithelium (RPE; *Tgfbr2*$^{\Delta eye}$ **top panel**, **arrowheads**), areas with a thickened (*Tgfbr2*$^{\Delta eye}$ **middle panel**) and thinned (*Tgfbr2*$^{\Delta eye}$ **bottom panel**) RPE, and an accumulation of pigmented cells in the sensory retina (*Tgfbr2*$^{\Delta eye}$ **top**, **middle**, and **bottom panels**, **arrows**). **C:** Detailed magnification of the retina. In the *Tgfbr2*$^{\Delta eye}$ mouse, the retina is degenerated, with a complete loss of photoreceptors. The RPE is disorganized, pigmented cells accumulate in the sensory retina, and the choroid is thickened. **D:** *In vivo* funduscopy and fluorescein angiography of the control animal are normal. *Tgfbr2*$^{\Delta eye}$ mice show a hyperpigmented fundus (**middle panels**) or retinal detachment (**right panels**). Diameters of the image sections refer to 2 mm retina. Scale bars: 500 μm (**A**); 20 μm (**B**); 50 μm (**C**). INL, inner nuclear layer; IPL, inner plexiform layer; PS, photoreceptor segment; RGC, retinal ganglion cell.

Expression of Angiogenic Factors and Immune Modulating Cytokines in *Tgfbr2*$^{\Delta eye}$ Mice

The immunovascular axis, a cross talk of the RPE with immune and vascular cells, is considered a potent driver of CNV formation.[4] To clarify the mechanisms behind CNV induced by TβRII deletion, we consequently analyzed the mRNA expression levels of immune-modulating cytokines and markers for the reactivity of Müller glia and microglia cells, respectively. Early-induced *Tgfbr2*$^{\Delta eye}$ mice showed a significant increase in retinal mRNA expression levels of glial fibrillary acidic protein, Cd68, inducible nitric oxide synthase, Il-6, tumor necrosis factor-α, and monocyte chemoattractant protein-1 [chemokine (C-C motif) ligand 2] at the age of 6 weeks compared to control littermates (Figure 6A). However, in 3-month—old late-induced *Tgfbr2*$^{\Delta eye}$ mice, the retinal mRNA expression levels were not significantly enhanced compared to controls; in fact, glial fibrillary acidic protein was even significantly downregulated (Figure 6B). Next, we used an antibody against F4/80 to label macrophages and microglia cells.[49–51] The number of F4/80-positive cells was significantly ($P \leq 0.05$) increased in the choroid of early-induced *Tgfbr2*$^{\Delta eye}$ animals (142.67 ± 17.13, $n = 3$) when compared with controls (95.0 ± 8.40, $n = 4$) (Figure 6C). The F4/80-positive cells were detected in the subretinal space in close association with the CNV (Figure 6C). Furthermore, the number of F4/80-positive cells in the retina was significantly increased ($P \leq 0.001$) in early-induced *Tgfbr2*$^{\Delta eye}$ animals (145.75 ± 9.73, $n = 4$) compared to controls (22.5 ± 1.71, $n = 4$). Similarly, 3-month—old late-induced *Tgfbr2*$^{\Delta eye}$ animals also presented a distinct accumulation of F4/80-positive cells in the choroid when compared to controls (Figure 6D). Subsequently, we focused on molecular factors that influence vascular proliferation. In our previously published study, we already showed that early-induced

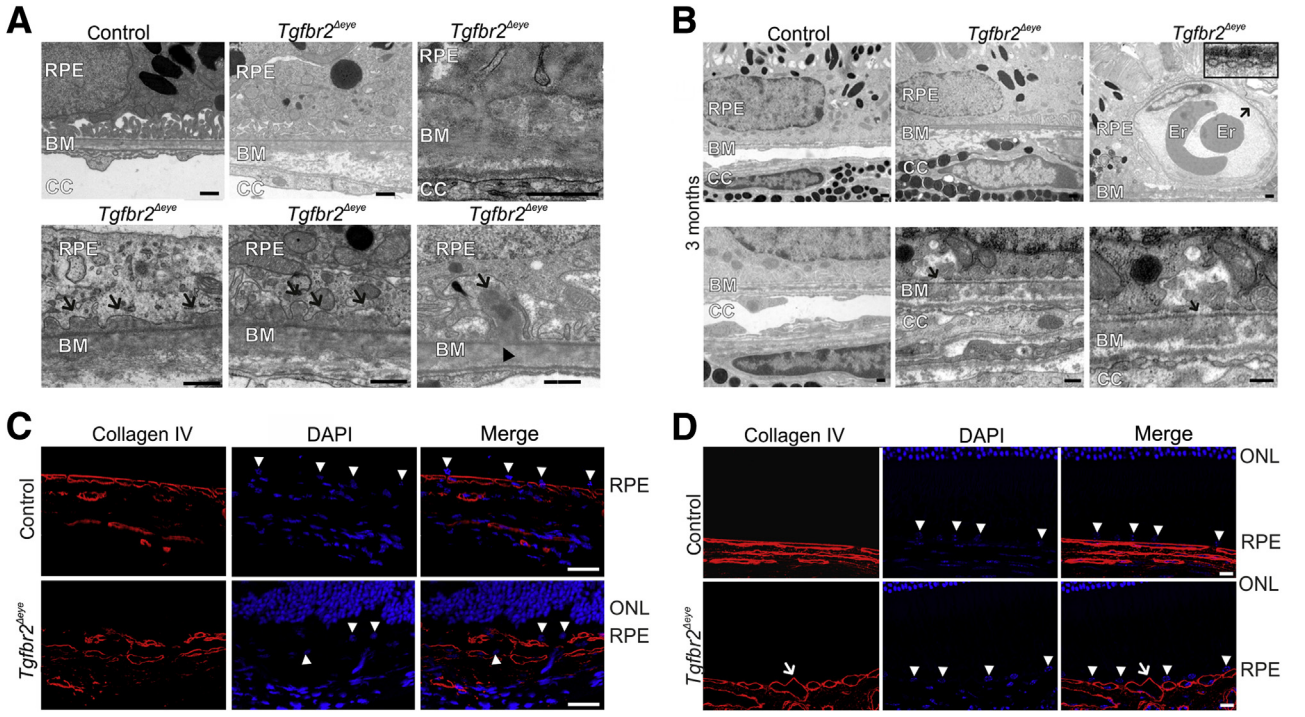

Figure 5 Structural changes of the Bruch membrane (BM) in early- and late-induced *Tgfbr2*$^{\Delta eye}$ mice. **A:** Transmission electron microscopy (TEM) of retinal pigment epithelium (RPE)/BM in early-induced 2.5-month—old mice. **Top panels:** The BM of the control is of regular structure, but thickened in *Tgfbr2*$^{\Delta eye}$ mice as a result of an accumulation of collagen fibers and fine fibrillar extracellular material between the basal lamina of the choriocapillaris (CC) and the elastic layer of the BM. In some areas (**right panels**), the RPE basal lamina is replaced by polymorphous electron-dense material that reaches from the elastic layer of the BM to the RPE basal infoldings. **Bottom panels:** In other RPE/BM areas of early-induced *Tgfbr2*$^{\Delta eye}$ mice, irregular nodules arise from the RPE basal lamina (**arrows**) and extend between the basal infoldings of the RPE. In places (**arrowhead**, **right panel**), the RPE basal lamina is interrupted where nodules arise. **B:** TEM of RPE/BM in 3-month—old late-induced *Tgfbr2*$^{\Delta eye}$ mice. RPE/BM are of regular structure in control mice, but thickened in *Tgfbr2*$^{\Delta eye}$ mice. Erythrocyte (Er)—filled vessels with fenestrated endothelium (**arrow**) are seen between RPE and photoreceptor outer segments (**top right panel**, **inset**). In places, the RPE basal lamina is interrupted (**arrow**) and electron-dense nodules arise to extend between the basolateral RPE infoldings (**bottom middle panel**). Higher magnification is given (**bottom right panel**). **C:** Immunoreactivity for collagen IV (red) of the retinal/choroidal interface in early-induced, 4-week—old *Tgfbr2*$^{\Delta eye}$ mice. In the control, the basal laminae of RPE and choriocapillaris endothelium are labeled. In *Tgfbr2*$^{\Delta eye}$ mice, staining is seen in the basal lamina of the choriocapillaris. Staining is irregular and patchy in the region of the RPE. Nuclei are DAPI stained (blue). RPE nuclei are marked by **arrowheads**. **D:** Immunoreactivity for collagen IV (red) in the retinal/choroidal interface in late-induced, 3-month—old *Tgfbr2*$^{\Delta eye}$ mice. In the control, the basal laminae of RPE and choriocapillaris endothelium are continuously labeled. In *Tgfbr2*$^{\Delta eye}$ mice, labeling is seen in the basal lamina surrounding choriocapillaris vessels, but is incomplete underneath the RPE. In places, the vascular basal lamina continues between RPE cells (**arrows**), indicating areas of choroidal neovascularization. Nuclei are DAPI stained (blue). RPE nuclei are marked by **arrowheads**. Scale bars: 500 nm (**A** and **B**, **top panels**); 250 nm (**B**, **bottom panels**); 50 μm (**C** and **D**). ONL, outer nuclear layer.

4-week—old *Tgfbr2*$^{\Delta eye}$ mice had significantly elevated mRNA expression levels for the angiogenic factors Vegf-a 120, Vegf-a 164, fibroblast growth factor-2, insulin growth factor-1, angiopoetin 2, and platelet-derived growth factor-b compared to control littermates.[21] We now performed immunohistochemistry for VEGF-A to localize the increased levels in the retina of early-induced *Tgfbr2*$^{\Delta eye}$ mice (Figure 6E). Although VEGF-A immunoreactivity was not detectable in control eyes, there was distinct and intense staining of the ganglion cell layer of early-induced *Tgfbr2*$^{\Delta eye}$ mice. When we screened the retinas of late-induced *Tgfbr2*$^{\Delta eye}$ mice and their control littermates for the expression levels of the Vegf-a isoforms 120 and 164, the expression of Vegf-a 120 was not altered, whereas the expression of Vegf-a 164 was significantly reduced in 5-week—old late-induced *Tgfbr2*$^{\Delta eye}$ mice compared to controls (Figure 6F). However, at the age of 6 months, the retinal expression levels of both Vegf-a 120 and 164 were significantly higher in late-induced *Tgfbr2*$^{\Delta eye}$ mice compared to controls. Overall, angiogenic and immune reactivities were much higher in early-induced than in late-induced *Tgfbr2*$^{\Delta eye}$ mice.

Formation of Basal Lamina Deposits in *Tgfbr2*$^{\Delta eye}$ Mice

Because CNVs need to find their way across BM and through the RPE barrier, we used transmission electron microscopy to analyze the structure of both. Control mice showed the regular, five-layered architecture of the BM (Figure 5, A and B). In early- and late-induced *Tgfbr2*$^{\Delta eye}$ mice, the BM had thickened as the result of an accumulation of collagen fibers and fine fibrillar extracellular material was detected between the basal lamina of the choriocapillaris and the elastic layer of the BM (Figure 5, A and B).

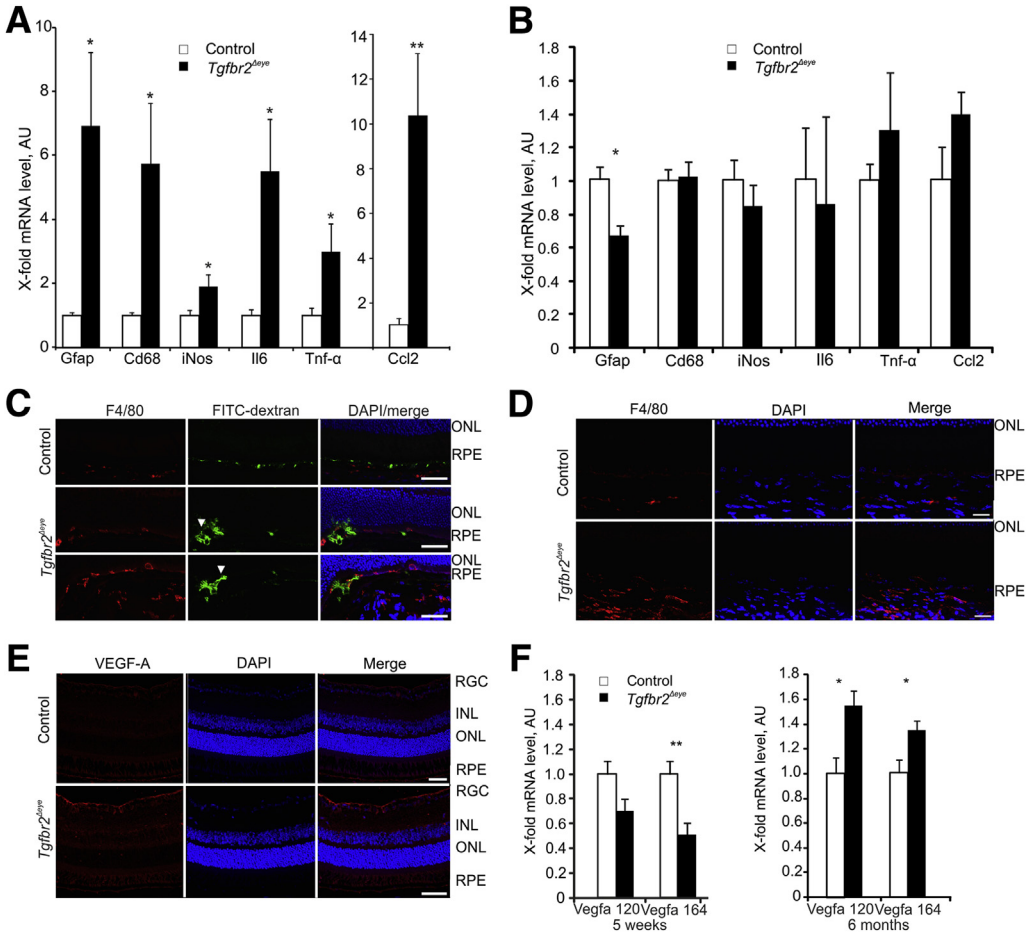

Figure 6 Expression of angiogenic and immune-modulating molecules in early- and late-induced *Tgfbr2*$^{\Delta eye}$ mice. **A** and **B:** Real-time RT-PCR for mRNA of glial fibrillary acidic protein (Gfap), Cd68, inducible nitric oxide synthase (iNos), chemokine (C-C motif) ligand 2 (Ccl2), Il-6, and tumor necrosis factor-α (Tnf-α) in 6-week–old early-induced (**A**) and 5-week–old late-induced (**B**) *Tgfbr2*$^{\Delta eye}$ mice and controls. **C:** Fluorescein isothiocyanate (FITC)–dextran (green)–perfused and F4/80 (red)–immunostained sections of a 6-week–old early-induced *Tgfbr2*$^{\Delta eye}$ mouse and control. The control mouse shows weak immunoreactivity for F4/80 (red)–positive cells in the choroid. In *Tgfbr2*$^{\Delta eye}$ mice, the choroidal immunoreactivity for F4/80 (red) is more pronounced, and numerous F4/80-positive cells accumulate in the subretinal space and in close association to choroidal vessels penetrating the retinal pigment epithelium (RPE; **arrowhead**). Nuclei are DAPI stained (blue). **D:** F4/80 (red)–immunostained sections of a 3-month–old, late-induced *Tgfbr2*$^{\Delta eye}$ mouse and control. A weak signal for F4/80 is visible in the choroid of the control mouse. In contrast, the *Tgfbr2*$^{\Delta eye}$ mouse shows numerous F4/80-positive cells in the choroid. Nuclei are DAPI stained (blue). **E:** Immunoreactivity for vascular endothelial growth factor-A (VEGF-A; red) in early-induced 4-week–old mice. The control mouse has a faint immunoreactivity for VEGF-A, which is increased in the *Tgfbr2*$^{\Delta eye}$ mouse. Nuclei are DAPI stained (blue). **F:** Real-time RT-PCR for mRNA of Vegf-a 120 and Vegf-a 164 in late-induced 5-week–old mice (**left panel**) and 6-month–old mice (**right panel**). Data are expressed as means ± SEM (**A**, **B**, and **F**). $n \geq 7$ early-induced mice, control and *Tgfbr2*$^{\Delta eye}$ (**A**); $n \geq 6$ late-induced mice (5 weeks old), control (**B** and **F**); $n \geq 2$ late-induced mice (5 weeks old), *Tgfbr2*$^{\Delta eye}$ (**B** and **F**); $n = 9$ late-induced mice (6 months old), control (**F**); $n = 7$ late-induced mice (6 months old), *Tgfbr2*$^{\Delta eye}$ (**F**). $^{*}P \leq 0.05$, $^{**}P \leq 0.01$ (*t*-test). Scale bars: 50 μm (**C** and **E**); 20 μm (**D**). AU, arbitrary unit; INL, inner nuclear layer; ONL, outer nuclear layer; RGC, retinal ganglion cell.

Moreover, in some areas, the RPE basal lamina had been replaced by polymorphous electron-dense material that was localized between the elastic layer of the BM and the RPE basal infoldings (Figure 5A). In other areas of the same eye, irregular nodules arising from the RPE basal lamina and with comparable electron density were found between the basal infoldings of the RPE (Figure 5A). In addition, the basal lamina was frequently found to be interrupted where nodules arised (Figure 5, A and B). Nodules and RPE basal lamina interruptions were found frequently in early-induced mice and more rarely in late-induced mice. The changes were essentially similar in structure to basal lamina deposits typically found in CNV in humans patients with AMD. In addition, we found interruptions of the RPE basal lamina with an associated accumulation of electron-dense material in the adjacent RPE infoldings (Figure 5A). Next, we labeled the basal laminae of RPE and choriocapillaris by collagen type IV immunohistochemistry. In control mice, the basal laminae of both RPE and choriocapillaris endothelium were continuously labeled (Figure 5, C and D). In early-induced *Tgfbr2*$^{\Delta eye}$ mice, continuous staining was only seen in the basal lamina of the choriocapillaris. Staining was irregular and patchy in the region of the RPE (Figure 5C). In late-induced *Tgfbr2*$^{\Delta eye}$ mice, continuous labeling was seen in the basal lamina surrounding choriocapillaris vessels, but was incomplete underneath the RPE

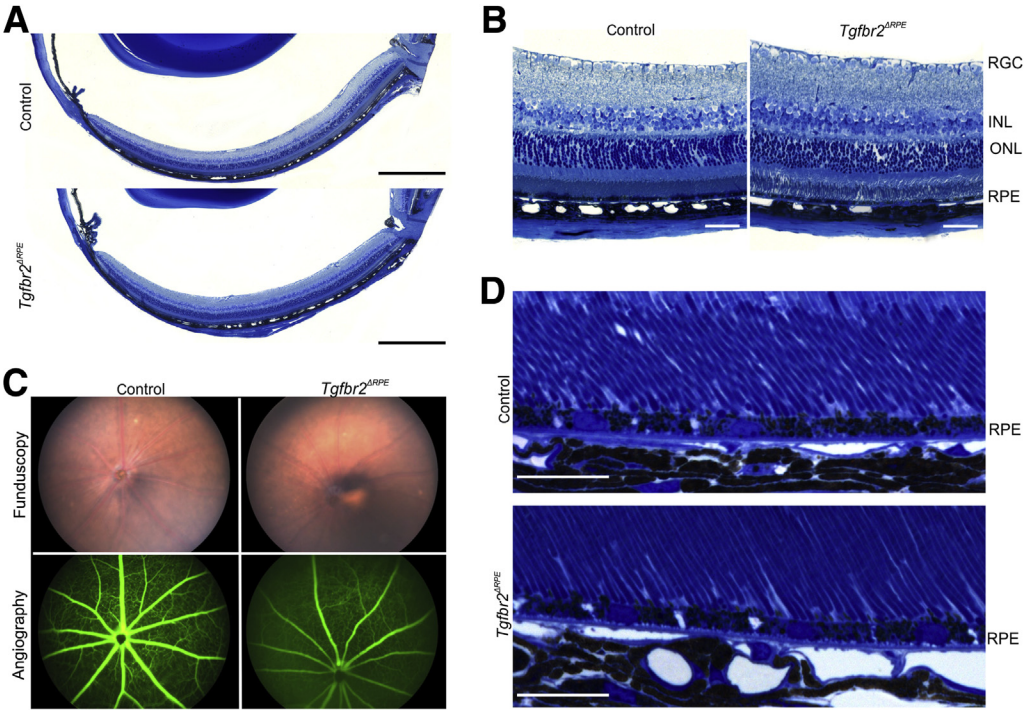

Figure 7 Deletion of transforming growth factor−β (TGF-β) signaling in the retinal pigment epithelium (RPE). Stained semithin sections, according to the method of Richardson et al.[37] **A:** Retinal hemispheres of 6-month−old animals. The control mouse and the *Tgfbr2*$^{\Delta RPE}$ mouse do not obviously differ in structure. **B:** Detailed magnification of retina/choroid in a *Tgfbr2*$^{\Delta RPE}$ mouse and its control littermate, showing an essentially normal morphology. **C:** *In vivo* funduscopy and fluorescein angiography show no obvious alterations in the *Tgfbr2*$^{\Delta RPE}$ mouse compared to the control. Diameters of the image sections refer to 2 mm retina. **D:** Detailed magnifications of the interface of the outer retina, RPE, and choroid, again showing a regular morphology in the *Tgfbr2*$^{\Delta RPE}$ mice and controls. Scale bars: 500 μm (**A**); 50 μm (**B**); 20 μm (**D**). INL, inner nuclear layer; ONL, outer nuclear layer; RGC, retinal ganglion cell.

(Figure 5D). In places, the vascular basal lamina reached between RPE cells, indicating areas of CNV formation.

Cell-Specific Conditional Deletion of *Tgfbr2* in the RPE and Vascular Endothelium

Next, we aimed at identifying the specific cell type that is responsible for CNV in *Tgfbr2*$^{\Delta eye}$ mice. We focused on the RPE and the vascular endothelium, as endothelial proliferation and breakdown of the RPE barrier are essential requirements for CNV formation. To this end, we generated *Tgfbr2*$^{\Delta RPE}$ mice with a *Tgfbr2* deletion specifically in the RPE via doxycycline-driven RPE-specific expression of Cre recombinase. Successful RPE-specific TβRII deletion was confirmed by immunohistochemistry. Control animals showed immunoreactivity for TβRII in photoreceptor outer segments, RPE, and choroid. In contrast, immunoreactivity for TβRII in the RPE was not detectable in the RPE of *Tgfbr2*$^{\Delta RPE}$ mice (Supplemental Figure S2C). In addition, we confirmed recombination by PCR (Supplemental Figure S2D). The ocular morphology of *Tgfbr2*$^{\Delta RPE}$ mice was analyzed in detail by using essentially similar methods as used for *Tgfbr2*$^{\Delta eye}$ mice, but neither choroidal CNV nor other obvious structural changes were detected (Figure 7, A−D). For generation of *Tgfbr2*$^{\Delta EC}$ mice with specific deletion of TβRII in vascular endothelial cells, *VeCad-Cre-ER*^{T2} mice were used with endothelial-specific tamoxifen-inducible Cre expression. Specific recombination in retinal and choroidal vessels was confirmed by green fluorescent protein immunoreactivity in *VeCad-Cre-ER*^{T2} crossed with *mT/mG* reporter mice (Supplemental Figure S2E). When analyzing the structure of 6-week−old *Tgfbr2*$^{\Delta EC}$ mice, the pronounced structural changes that we had reported[21] for early-induced *Tgfbr2*$^{\Delta eye}$ mice, such as retinal and vitreal neovascularization, retinal detachment, and vitreal hemorrhages, were completely absent (Figure 8, A and B). Still, similar to our results seen in early-induced *Tgfbr2*$^{\Delta eye}$ mice,[21] dilated vessels were frequently observed in the inner nuclear layer surrounded by electron-dense, extravascular material (Figure 8, C and E). Intriguingly, at the retinal/choroidal interface, focal areas were frequently observed in which photoreceptor outer segments were degenerated or absent, the RPE was multilayered, and vascular endothelial cells, together with extravasated erythrocytes, had accumulated in the subretinal space (Figure 8D). FITC-dextran−perfused ocular sections of *Tgfbr2*$^{\Delta EC}$ mice showed tracer leakage from the choriocapillaris toward the RPE and choroidal vessels penetrating the RPE, indicating a breakdown of the outer blood-retinal barrier and the formation of CNV (Figure 9A). In 4-week−old *Tgfbr2*$^{\Delta EC}$ animals and controls, the choroidal vessels were covered by neural/glial antigen 2−positive pericytes (data not shown). In contrast to

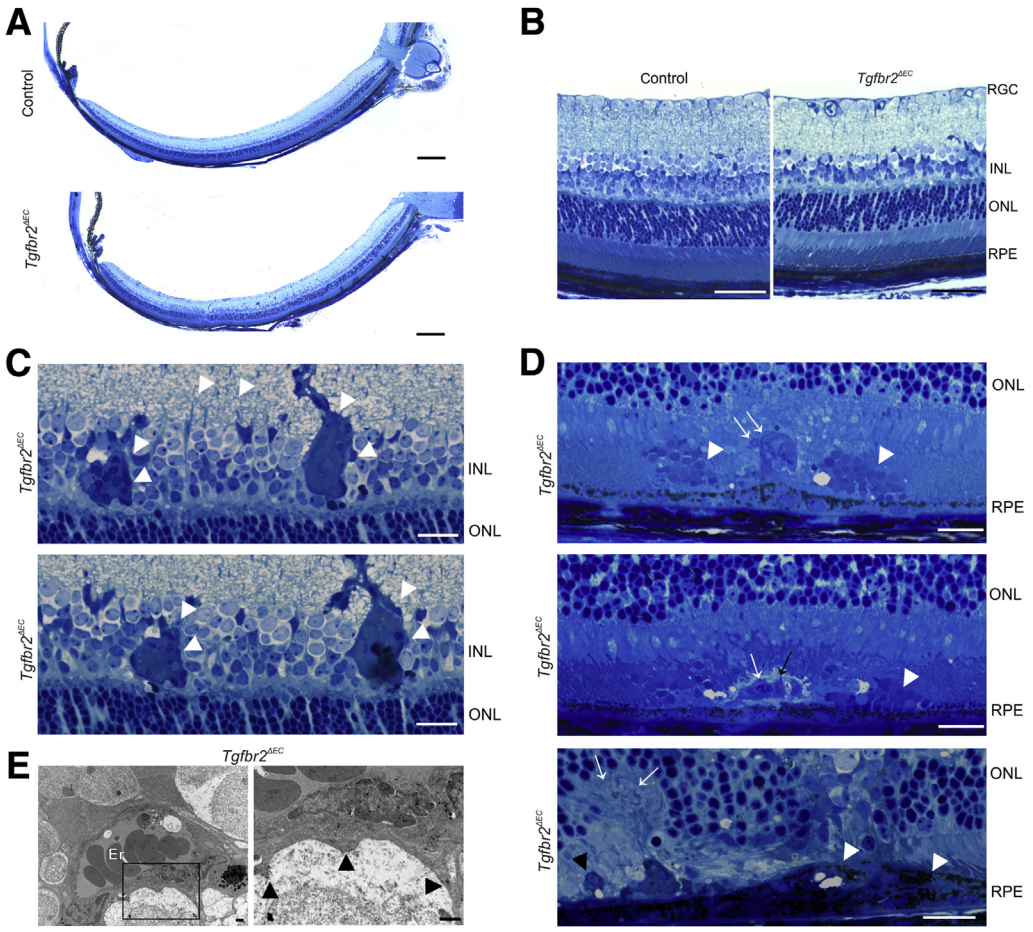

Figure 8 Structural changes of the retina in *Tgfbr2*$^{\Delta EC}$ mice. Stained semithin sections of a 6-week–old *Tgfbr2*$^{\Delta EC}$ mouse and its control littermate, according to the method of Richardson et al.[37] **A:** Retinal hemispheres of the control mouse and the *Tgfbr2*$^{\Delta EC}$ littermate. **B:** Detailed magnification of the retina and choroid. **C:** Dilated retinal vessels (**white arrowheads**) are seen in the inner nuclear layer (INL) of *Tgfbr2*$^{\Delta EC}$ mice. **D:** In the retinal/choroidal interface, endothelial cells (**white arrows**), erythrocytes (Ers; **white arrowheads**), mononuclear cells (**black arrowhead**), and ragged edged extravascular material (**black arrow**) are seen between degenerating photoreceptor outer segments. **E:** Transmission electron microscopy of an intraretinal vessel in a 6-week–old *Tgfbr2*$^{\Delta EC}$ animal. Electron-dense material is visible around the intraretinal vessel (**left panel**); the **boxed area** is shown in higher magnification (**right panel**). The **arrowheads** point to the electron-dense extravascular material with ragged edged appearance. Scale bars: 200 μm (**A**); 50 μm (**B**); 20 μm (**C** and **D**); 1000 nm (**E**). ONL, outer nuclear layer; RGC, retinal ganglion cell; RPE, retinal pigment epithelium.

our data from *Tgfbr2*$^{\Delta eye}$ mice, we did not observe an accumulation of F4/80-positive cells in the choroid of *Tgfbr2*$^{\Delta EC}$ mice (Figure 9B) (control: 95.0 ± 8.40, $n = 4$; *Tgfbr2*$^{\Delta EC}$: 111.67 ± 10.41, $n = 3$; $P \geq 0.05$). In contrast, F4/80-positive cells were increased in the retina (control: 22.5 ± 1.71, $n = 4$; *Tgfbr2*$^{\Delta EC}$: 108.0 ± 3.51, $n = 3$; $P \leq 0.001$). In addition, immunoreactivity for collagen IV in the RPE/BM region was seen in basal laminae of choriocapillaris and RPE and did not markedly differ between *Tgfbr2*$^{\Delta EC}$ mice and controls (Figure 9C). Transmission electron microscopy confirmed the findings seen by light microscopy and the presence of degenerated photoreceptor outer segments, multilayered RPE, and extravasated erythrocytes (Figure 9D). Moreover, plasma-derived electron-dense material did not pass the RPE tight junctions in controls but accumulated between RPE and photoreceptor outer segments in *Tgfbr2*$^{\Delta EC}$ mice, indicating breakdown of the RPE barrier (Figure 9E). Overall, our data obtained in *Tgfbr2*$^{\Delta EC}$ mice strongly support the conclusion that deletion of TβRII in vascular endothelial cells alone is sufficient to promote the formation of CNV.

Discussion

We conclude that the deletion of TGF-β signaling in the ocular microenvironment is sufficient to induce CNV and other phenotypic characteristics of AMD in humans. Lack of endothelial TGF-β signaling is sufficient to trigger the onset of CNV, whereas its lack in the RPE is not relevant in this context. This conclusion is based on the following: i) the generation of mice with TβRII deficiency in the entire microenvironment of the eye, in vascular endothelial cells, or in the RPE; ii) the frequent detection of capillaries with fenestrated, PLVAP-positive endothelium that originate from the choriocapillaris and traverse the RPE to

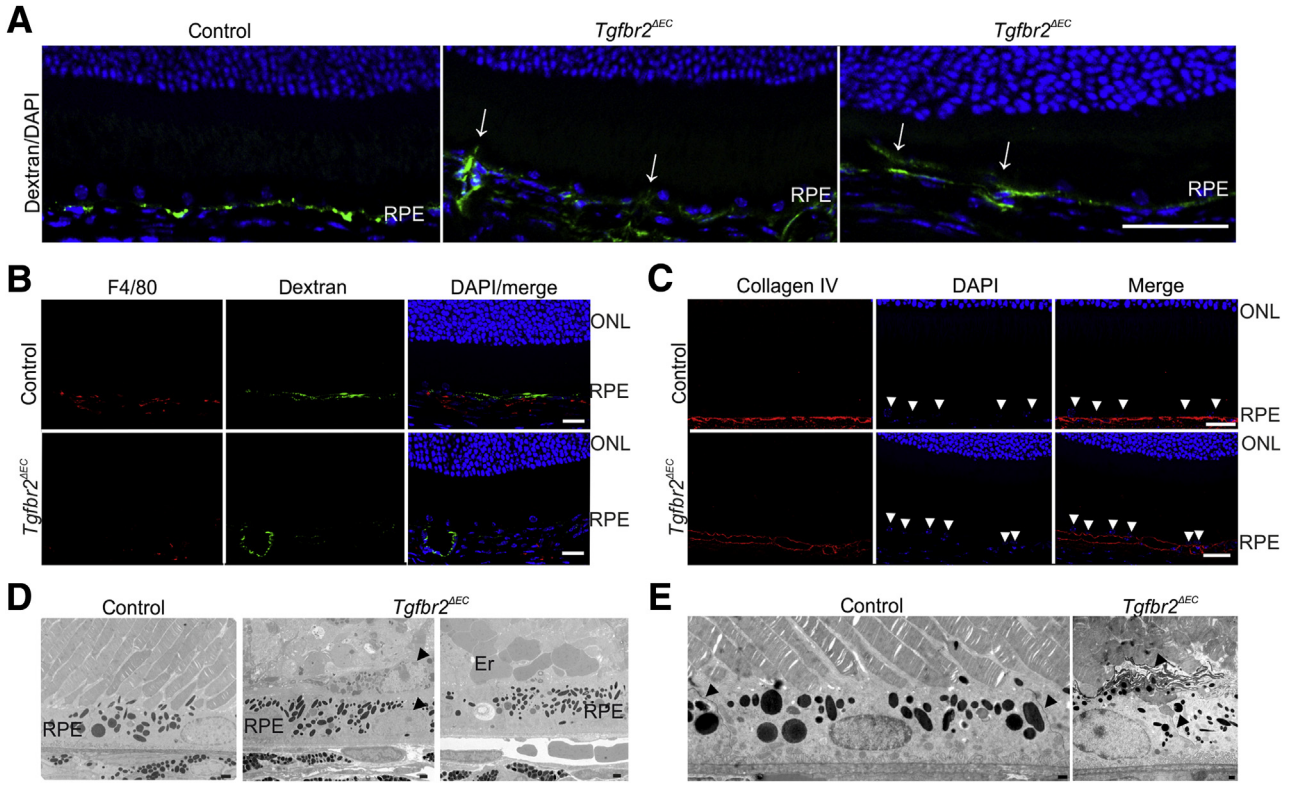

Figure 9 Structural changes of the retinal/choroidal interface in *Tgfbr2*$^{\Delta EC}$ mice. **A:** Fluorescein isothiocyanate (FITC)—dextran—perfused retinal meridional sections of a 6-week—old *Tgfbr2*$^{\Delta EC}$ mouse and its control littermate. **White arrows** point toward tracer leakage in the retinal pigment epithelium (RPE; **middle panel**) and choroidal vessels (**right panel**) invading the RPE. Nuclei are DAPI stained (blue). **B:** FITC-dextran (green)—perfused and F4/80 (red)—immunostained sections. The control and the *Tgfbr2*$^{\Delta EC}$ littermate show immunoreactivity for F4/80 (red)—positive cells in the choroid, which are not higher in number in the mutant. Nuclei are DAPI stained (blue). **C:** Immunoreactivity for collagen IV (red) in the RPE/Bruch membrane (BM) region of 6-week—old mice. Basal laminae of choriocapillaris and RPE are regularly labeled in control and mutant. Nuclei are DAPI stained (blue), and RPE nuclei are marked by **white arrowheads**. **D** and **E:** Transmission electron microscopy of RPE/BM in 4- to 6-week—old mice. **D:** In the control, photoreceptor outer segments, RPE, and BM are of normal structure. In the *Tgfbr2*$^{\Delta EC}$ mouse, areas of degenerated photoreceptor outer segments, multilayered RPE (**black arrowheads** point toward nuclei of RPE cells), and extravasated erythrocyte (Er) are present. **E:** Plasma-derived electron-dense material does not pass the RPE tight junctions in controls (**black arrowheads**). In contrast, in the mutant, it accumulates between RPE and photoreceptor outer segments (**black arrowheads**). Scale bars: 50 μm (**A**); 20 μm (**B** and **C**); 1000 nm (**D**); 500 nm (**E**). ONL, outer nuclear layer.

anastomose with retinal capillaries; iii) the presence of basal lamina—like deposits around the RPE basal infoldings and of areas with multilayered RPE; iv) the degeneration of photoreceptor outer segments; and v) the finding of distinct accumulations of F4/80-positive macrophages in the choroid.

TGF-β Functions at the Retinal/Choroidal Interface to Prevent CNV

The results of our study clearly support the concept that a major function of TGF-β signaling in choroid and retina is the stabilization of the choroidal and retinal vascular beds that are each essential for neuronal integrity in the sensory retina. This function includes the prevention of neoangiogenic processes in the two capillary beds that would otherwise cause neuronal dysfunction and death in the retina. It is of interest that the sensitivity to the induced lack of TGF-β signaling differs between the two vascular beds, as the formation of microaneurysms, leaky capillaries, and hemorrhages of the retinal vasculature is only seen when TGF-β signaling is deleted in the ocular microenvironment shortly after birth.[21] In contrast, the formation of CNV is seen regardless if TGF-β signaling is interfered with in newborn or 3- to 4-week—old animals. A likely explanation is the fact that the retinal vasculature of the mouse eye forms and differentiates in the first 2 weeks after birth[52] and may be more vulnerable to lack of TGF-β signaling during that period. A critical contributing factor may be the failure of pericyte differentiation around retinal capillaries that results from deficiency of TGF-β signaling during that period.[21] Formation of the choroidal vasculature is completed in late embryonic life, and the choriocapillaris is mature at birth.[53]

The coating of the choroidal vessels with neural/glial antigen 2—positive pericytes in early- and late-induced *Tgfbr2*$^{\Delta eye}$ and *Tgfbr2*$^{\Delta EC}$ animals was comparable to controls, which appears to indicate that lack of pericyte presence or differentiation is not a requirement for CNV. Data from genetically modified mice with a specific

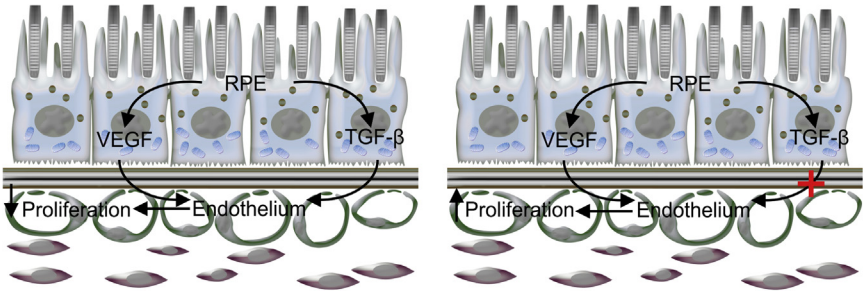

Figure 10 Schematic of signaling events at the retinal-choroidal interface. **Left panel:** Normally, the retinal pigment epithelium (RPE) secretes high amounts of both transforming growth factor—β (TGF-β) and vascular endothelial growth factor (VEGF) that both ensure an appropriate physiological microenvironment for the choriocapillaris, including its VEGF-mediated maintenance, and TGF-β—mediated inhibition of proliferation. **Right panel:** The deletion of *Tgfbr2* in endothelial cells results in the specific disability of TGF-β to act on endothelial cells (**red cross**). This results in an imbalance of the effects of VEGF/TGF-β, a scenario that promotes the proliferation of the vascular endothelium of the choriocapillaris in the direction of the RPE and, finally, results in choroidal neovascularization.

deficiency of platelet-derived growth factor-B in endothelial cells further challenge the role of pericytes in the formation of CNV as these mice show a varying degree of pericyte loss without developing CNV.[54] The higher sensitivity of the choriocapillaris to lack of TGF-β signaling, as opposed to the mature retinal vasculature, may also be caused by the presence of the high amounts of VEGF at the retinal/choroidal interface that are continuously secreted by the RPE, the only source of VEGF in the back of the adult eye.[55] Secretion of VEGF occurs in a polarized manner to the RPE basolateral side facing the choriocapillaris[56,57] and is expected to convey a proliferative signal to endothelial cells of the choriocapillaris that are no more under the influence of constitutive TGF-β signaling in animals with a deletion of TβRII.

TGF-β and VEGF as Part of a Homeostatic System to Maintain Integrity of the Choriocapillaris

Not only VEGF but also TGF-β1 and TGF-β2 are present at high amounts at the retinal/choroidal interface.[20] It is tempting to speculate that both factors are critical parts of a homeostatic system designed to maintain structure and function of the choriocapillaris. In this system, VEGF would be required to maintain the extreme high density of the choriocapillaris and its fenestrations,[57,58] whereas TGF-βs antagonize any proliferative properties of VEGF signaling on the vascular endothelium. Failure in the balance of this homeostatic system would cause ablation of the choriocapillaris or induce its proliferation, finally leading to CNV (Figure 10). There is direct evidence for such a homeostatic system from studies in genetically engineered mice in which lack of VEGF and/or increase in TGF-β activity leads to ablation of the choriocapillaris,[14–18] whereas an increase in VEGF[59,60] and/or a lack of TGF-β activity (results of our present study) have direct opposite and proliferative effects. For the initiation of CNV, lack of TGF-β activity appears to be more relevant than sole increase of VEGF activity, as mice with overexpression of VEGF in the RPE develop an intrachoroidal neovascularization, but no CNV.[59,60] VEGF and TGF-βs induce the transcription of one another in multiple cell types[61–66] and may well do so in the RPE, establishing an autoregulatory feedback system designed to maintain structure and function of the choriocapillaris. We realize that this concept needs to be validated in further studies that should also aim at a complete identification of the signaling network that drives endothelial proliferation and CNV formation downstream of TGF-β signaling deficiency.

Potential Neuroprotective Effects of TGF-β

Late-induced $Tgfbr2^{\Delta eye}$ mice showed a dramatic deterioration of the retina. The prolonged presence and formation of CNV, and its detrimental effects on structure and function of the retina, may explain this finding. It may also indicate a participation of TGF-β signaling in a neuroprotective pathway independent of the formation of CNV. We recently showed that TGF-β signaling protects retinal neurons from developmental programmed cell death.[33] It is well possible that it also contributes to maintenance of adult neurons by protecting them from apoptosis. In support of such a scenario are findings reported by Walshe et al,[67] who neutralized TGF-β in the adult mouse eye via expression of soluble endoglin, a TGF-β inhibitor. Apoptosis of retinal ganglion cells was observed, as were functional deficits detected by ERG. Neuroprotective activities of TGF-βs were reported for multiple types of neurons throughout the central nervous system, such as in the striatum,[68] spinal cord,[69] substantia nigra,[70] or hippocampus.[71] Similarly, there is increasing evidence that VEGF signaling is important for the trophic maintenance of neurons and their survival after injury, effects that appear to be mediated via the VEGF receptor-2.[72–76] Mice with a constitutive high expression of VEGF in retinal ganglion cells are protected from retinal ganglion cell degeneration after axotomy via VEGF receptor-2 and downstream activation of extracellular signal—regulated kinase 1/2 and Akt pathways.[77] Although TGF-β/VEGF are antagonists in their actions at the retinal/choroidal interface and the choriocapillaris, they

may cooperate in their neuroprotective activities. Both functions would serve the ultimate goal to maintain structure and function of the retina.

The Formation of BlamD-Like Material Is Not Required for CNV

Although CNV was consistently observed in the eyes of both early- and late-induced *Tgfbr2*$^{\Delta eye}$ mice, and in those of *Tgfbr2*$^{\Delta EC}$ mice, other findings were predominant only in the eyes of early-induced *Tgfbr2*$^{\Delta eye}$ mice. This includes the formation of homogeneous extracellular material between the basal infoldings of the RPE and internal to the RPE basal lamina. The material was similar in electron density and structure to that of basal lamina deposits (BlamDs), a characteristic finding in patients with early age-related macular degeneration.[78–80] BlamD-like changes were commonly observed in early-induced *Tgfbr2*$^{\Delta eye}$ mice, only rarely observed in late-induced *Tgfbr2*$^{\Delta eye}$ mice, and not observed in *Tgfbr2*$^{\Delta EC}$ mice, suggesting that they are not a requirement for CNV and breakdown of the RPE barrier. Our immunohistochemical data indicate that the homogeneous extracellular BlamD-like material contains collagen type IV, an observation that correlates with the observation that basal lamina proteins (eg, collagen IV and laminin) are present in BlamDs in human patients with AMD.[78,81] BlamD formation in AMD is likely caused by RPE dysfunction.[79] A comparable dysfunction might more easily happen in early-induced *Tgfbr2*$^{\Delta eye}$ mice, in which the RPE is not yet fully differentiated. Still, a common structural change of the RPE in our models with CNV was the loss of an epithelial monolayer and the formation of multilayered RPE cells. Beneath and above those multilayered RPE cells, newly formed vessels were observed, similar to type 1 (sub-RPE, occult) and type 2 (subretinal, classic) CNV in human patients. Direct deletion of TGF-β signaling in RPE cells appears not to be relevant for formation of BlamD-like material, as it was not observed in *Tgfbr2*$^{\Delta RPE}$ mice.

Neovascularization Is Associated with Macrophage Accumulation

A common finding in *Tgfbr2*$^{\Delta eye}$ mice with CNV was the marked accumulation of F4/80-positive macrophages in the region of the retinal/choroidal interface. Comparable findings have been described for patients experiencing AMD.[82] It is reasonable to assume that signaling molecules released from proliferative capillary endothelial cells attracted the cells. Reactive macrophages might contribute to the loss of the RPE barrier in our mice and its transition from an epithelial layer to a multilayer in areas of CNV. Our findings in *Tgfbr2*$^{\Delta RPE}$ mice indicate that lack TGF-β signaling in RPE cells is not required for this process. Currently, we do not know how proliferating choroidal endothelial cells manage to break through the RPE barrier, but we trust that our mouse models are appropriate tools to identify the causative molecular events. The expression of signaling molecules characteristic for reactive macrophages/microglia, such as inducible nitric oxide synthase, Il-6, tumor necrosis factor-α, and monocyte chemoattractant protein-1/chemokine (C-C motif) ligand, was elevated in the retinal mRNA of early-induced *Tgfbr2*$^{\Delta eye}$ mice, but not in late-induced mice. We attribute this observation to the marked changes in the inner retina of early-induced mice that are absent in late-induced mice. Still, those molecules might well be elevated in the microenvironment of the choroidal/retinal interface, where macrophages accumulate in mice with CNV.

TGF-β Signaling and Blood-Retinal Barrier

Leakage of high-mol. wt. FITC-dextran and erythrocytes into the retina and subretinal space, after induced TGF-β signaling deficiency, implicates disruption of the inner and outer blood retinal barriers. Deficiency of the TGF-β signaling pathway in endothelial cells is likely the major contributor in this scenario. Comparable, mice with an endothelial-specific deficiency of SMAD4, an intracellular downstream mediator of TGF-β signaling, or mice with a deletion of TβRII specifically in endothelial cells in the brain[83,84] show perinatal intracerebral hemorrhages and a breakdown of the blood-brain barrier. Furthermore, the virus-driven expression of soluble endoglin results in an inhibition of TGF-β1 signaling in the murine retina, a situation that also causes breakdown of the blood-retinal barrier, most likely mediated through a decreased association of the tight junction proteins occludin and zona occludens-1.[67]

TGF-β Signaling in Human Patients with AMD

Several independent case-control genome-wide association studies detected an association of two synonymous polymorphisms in exon 1 of the high-temperature requirement A1 (*HTRA1*) gene, with a high risk to develop AMD.[85–87] The gene product HTRA1 appears to play a causative role in CNV.[88–90] Intriguingly, a recent study provided evidence that the two synonymous HTRA1 variants influence their protein interaction with TGF-β1, leading to an impaired regulation of TGF-β signaling.[91] Moreover, a collaborative genome-wide association study identified *TGFBR1*, the gene encoding for the TGF-β1 type I receptor, as a new susceptibility gene for AMD, further highlighting the importance of the TGF-β signaling pathway in the context of AMD.[85]

Conclusion

Our findings emphasize the importance of TGF-β signaling as a key player in the development of ocular neovascularization and implicate a fundamental role of TGF-β signaling in the pathogenesis of AMD. A more thorough understanding of this role at the retinal/choroidal interface has the distinct potential to lead to the development of novel

treatments strategies preventing CNV in patients experiencing AMD.

Acknowledgments

We thank Elke Stauber, Margit Schimmel, Angelika Pach, Silvia Babl, and Elfriede Eckert for their excellent technical assistance; and Antje Zenker for drawing the schematic of Figure 10.

A.S., S.V.L., and B.M.B. performed most of the experiments; A.S., S.V.L., B.M.B., and E.R.T. interpreted the data; H.J. and A.F. conducted *in vivo* angiography, three-dimensional imaging, and electroretinographic experiments; A.S., B.M.B., and E.R.T. wrote the manuscript; and B.M.B. and E.R.T. designed the research studies.

Supplemental Data

Supplemental material for this article can be found at *http://dx.doi.org/10.1016/j.ajpath.2017.06.018*.

References

1. Friedman DS, O'Colmain BJ, Muñoz B, Tomany SC, McCarty C, de Jong PTVM, Nemesure B, Mitchell P, Kempen J; Eye Diseases Prevalence Research Group: Prevalence of age-related macular degeneration in the United States. Arch Ophthalmol 2004, 122:564–572
2. Finger RP, Fimmers R, Holz FG, Scholl HPN: Incidence of blindness and severe visual impairment in Germany: projections for 2030. Invest Ophthalmol Vis Sci 2011, 52:4381–4389
3. Klaver CC, Wolfs RC, Vingerling JR, Hofman A, de Jong PT: Age-specific prevalence and causes of blindness and visual impairment in an older population: the Rotterdam Study. Arch Ophthalmol 1998, 116:653–658
4. Ambati J, Fowler BJ: Mechanisms of age-related macular degeneration. Neuron 2012, 75:26–39
5. Lim LS, Mitchell P, Seddon JM, Holz FG, Wong TY: Age-related macular degeneration. Lancet 2012, 379:1728–1738
6. Fritsche LG, Igl W, Bailey JNC, Grassmann F, Sengupta S, Bragg-Gresham JL, et al: A large genome-wide association study of age-related macular degeneration highlights contributions of rare and common variants. Nat Genet 2016, 48:134–143
7. Bhutto I, Lutty G: Understanding age-related macular degeneration (AMD): relationships between the photoreceptor/retinal pigment epithelium/Bruch's membrane/choriocapillaris complex. Mol Aspects Med 2012, 33:295–317
8. van Lookeren Campagne M, LeCouter J, Yaspan BL, Ye W: Mechanisms of age-related macular degeneration and therapeutic opportunities. J Pathol 2014, 232:151–164
9. Miller JW, Le Couter J, Strauss EC, Ferrara N: Vascular endothelial growth factor a in intraocular vascular disease. Ophthalmology 2013, 120:106–114
10. Miller JW: Age-related macular degeneration revisited–piecing the puzzle: the LXIX Edward Jackson memorial lecture. Am J Ophthalmol 2013, 155:1–35.e13
11. Kur J, Newman EA, Chan-Ling T: Cellular and physiological mechanisms underlying blood flow regulation in the retina and choroid in health and disease. Prog Retin Eye Res 2012, 31:377–406
12. Bill A, Törnquist P, Alm A: Permeability of the intraocular blood vessels. Trans Ophthalmol Soc U K 1980, 100:332–336
13. Ford KM, Saint-Geniez M, Walshe T, Zahr A, D'Amore PA: Expression and role of VEGF in the adult retinal pigment epithelium. Invest Ophthalmol Vis Sci 2011, 52:9478–9487
14. Kurihara T, Westenskow PD, Bravo S, Aguilar E, Friedlander M: Targeted deletion of Vegfa in adult mice induces vision loss. J Clin Invest 2012, 122:4213–4217
15. Marneros AG, Fan J, Yokoyama Y, Gerber HP, Ferrara N, Crouch RK, Olsen BR: Vascular endothelial growth factor expression in the retinal pigment epithelium is essential for choriocapillaris development and visual function. Am J Pathol 2005, 167:1451–1459
16. Le Y-Z, Bai Y, Zhu M, Zheng L: Temporal requirement of RPE-derived VEGF in the development of choroidal vasculature. J Neurochem 2010, 112:1584–1592
17. Saint-Geniez M, Kurihara T, Sekiyama E, Maldonado AE, D'Amore PA: An essential role for RPE-derived soluble VEGF in the maintenance of the choriocapillaris. Proc Natl Acad Sci U S A 2009, 106:18751–18756
18. Ohlmann A, Scholz M, Koch M, Tamm ER: Epithelial-mesenchymal transition of the retinal pigment epithelium causes choriocapillaris atrophy. Histochem Cell Biol 2016, 146:769–780
19. Strauss O: The retinal pigment epithelium in visual function. Physiol Rev 2005, 85:845–881
20. Pfeffer BA, Flanders KC, Guérin CJ, Danielpour D, Anderson DH: Transforming growth factor beta 2 is the predominant isoform in the neural retina, retinal pigment epithelium-choroid and vitreous of the monkey eye. Exp Eye Res 1994, 59:323–333
21. Braunger BM, Leimbeck SV, Schlecht A, Volz C, Jägle H, Tamm ER: Deletion of ocular transforming growth factor β signaling mimics essential characteristics of diabetic retinopathy. Am J Pathol 2015, 185:1749–1768
22. Mattapallil MJ, Wawrousek EF, Chan C-C, Zhao H, Roychoudhury J, Ferguson TA, Caspi RR: The Rd8 mutation of the Crb1 gene is present in vendor lines of C57BL/6N mice and embryonic stem cells, and confounds ocular induced mutant phenotypes. Invest Ophthalmol Vis Sci 2012, 53:2921–2927
23. Chytil A, Magnuson MA, Wright CVE, Moses HL: Conditional inactivation of the TGF-beta type II receptor using Cre:Lox. Genesis 2002, 32:73–75
24. Hayashi S, McMahon AP: Efficient recombination in diverse tissues by a tamoxifen-inducible form of Cre: a tool for temporally regulated gene activation/inactivation in the mouse. Dev Biol 2002, 244:305–318
25. Le Y-Z, Zheng W, Rao P-C, Zheng L, Anderson RE, Esumi N, Zack DJ, Zhu M: Inducible expression of cre recombinase in the retinal pigmented epithelium. Invest Ophthalmol Vis Sci 2008, 49:1248–1253
26. Monvoisin A, Alva JA, Hofmann JJ, Zovein AC, Lane TF, Iruela-Arispe ML: VE-cadherin-CreERT2 transgenic mouse: a model for inducible recombination in the endothelium. Dev Dyn 2006, 235:3413–3422
27. Boneva SK, Groß TR, Schlecht A, Schmitt SI, Sippl C, Jägle H, Volz C, Neueder A, Tamm ER, Braunger BM: Cre recombinase expression or topical tamoxifen treatment do not affect retinal structure and function, neuronal vulnerability or glial reactivity in the mouse eye. Neuroscience 2016, 325:188–201
28. Feil R, Brocard J, Mascrez B, LeMeur M, Metzger D, Chambon P: Ligand-activated site-specific recombination in mice. Proc Natl Acad Sci U S A 1996, 93:10887–10890
29. Schlecht A, Leimbeck SV, Tamm ER, Braunger BM: Tamoxifen-containing eye drops successfully trigger Cre-mediated recombination in the entire eye. Adv Exp Med Biol 2016, 854:495–500
30. Muzumdar MD, Tasic B, Miyamichi K, Li L, Luo L: A global double-fluorescent Cre reporter mouse. Genesis 2007, 45:593–605
31. Soriano P: Generalized lacZ expression with the ROSA26 Cre reporter strain. Nat Genet 1999, 21:70–71
32. Baulmann DC, Ohlmann A, Flügel-Koch C, Goswami S, Cvekl A, Tamm ER: Pax6 heterozygous eyes show defects in chamber angle

differentiation that are associated with a wide spectrum of other anterior eye segment abnormalities. Mech Dev 2002, 118:3−17
33. Braunger BM, Pielmeier S, Demmer C, Landstorfer V, Kawall D, Abramov N, Leibinger M, Kleiter I, Fischer D, Jägle H, Tamm ER: TGF-β signaling protects retinal neurons from programmed cell death during the development of the mammalian eye. J Neurosci 2013, 33: 14246−14258
34. Karnovsky MJ: A formaldehyde-glutaraldehyde fixative of high osmolarity for use in electron microscopy. J Cell Biol 1965, 27: 137−138
35. Kugler M, Schlecht A, Fuchshofer R, Kleiter I, Aigner L, Tamm ER, Braunger BM: Heterozygous modulation of TGF-β signaling does not influence Müller glia cell reactivity or proliferation following NMDA-induced damage. Histochem Cell Biol 2015, 144:443−455
36. Kugler M, Schlecht A, Fuchshofer R, Schmitt SI, Kleiter I, Aigner L, Tamm ER, Braunger BM: SMAD7 deficiency stimulates Müller progenitor cell proliferation during the development of the mammalian retina. Histochem Cell Biol 2017, 148:21−32
37. Richardson KC, Jarett L, Finke EH: Embedding in epoxy resins for ultrathin sectioning in electron microscopy. Stain Technol 1960, 35: 313−323
38. Braunger BM, Ohlmann A, Koch M, Tanimoto N, Volz C, Yang Y, Bösl MR, Cvekl A, Jägle H, Seeliger MW, Tamm ER: Constitutive overexpression of Norrin activates Wnt/β-catenin and endothelin-2 signaling to protect photoreceptors from light damage. Neurobiol Dis 2013, 50:1−12
39. Braunger BM, Ademoglu B, Koschade SE, Fuchshofer R, Gabelt BT, Kiland JA, Hennes-Beann EA, Brunner KG, Kaufman PL, Tamm ER: Identification of adult stem cells in Schwalbe's line region of the primate eye. Invest Ophthalmol Vis Sci 2014, 55:7499−7507
40. Wickham H: ggplot2, Elegant Graphics for Data Analysis. New York, NY, Springer, 2009
41. Livak KJ, Schmittgen TD: Analysis of relative gene expression data using real-time quantitative PCR and the 2(-Delta Delta C(T)) Method. Methods 2001, 25:402−408
42. Ertürk A, Becker K, Jährling N, Mauch CP, Hojer CD, Egen JG, Hellal F, Bradke F, Sheng M, Dodt H-U: Three-dimensional imaging of solvent-cleared organs using 3DISCO. Nat Protoc 2012, 7: 1983−1995
43. Committee for the Update of the Guide for the Care and Use of Laboratory Animals; National Research Council: Guide for the Care and Use of Laboratory Animals: Eighth Edition. Washington, DC, National Academies Press, 2011
44. Kaufman PL, Adler FH, Levin LA, Alm A: Adler's Physiology of the Eye. St. Louis, MO: Elsevier Health Sciences, 2011
45. Stan RV, Arden KC, Palade GE: cDNA and protein sequence, genomic organization, and analysis of cis regulatory elements of mouse and human PLVAP genes. Genomics 2001, 72:304−313
46. Stan R-V, Kubitza M, Palade GE: PV-1 is a component of the fenestral and stomatal diaphragms in fenestrated endothelia. Proc Natl Acad Sci U S A 1999, 96:13203−13207
47. Stan RV, Tse D, Deharvengt SJ, Smits NC, Xu Y, Luciano MR, McGarry CL, Buitendijk M, Nemani KV, Elgueta R, Kobayashi T, Shipman SL, Moodie KL, Daghlian CP, Ernst PA, Lee H-K, Suriawinata AA, Schned AR, Longnecker DS, Fiering SN, Noelle RJ, Gimi B, Shworak NW, Carrière C: The diaphragms of fenestrated endothelia: gatekeepers of vascular permeability and blood composition. Dev Cell 2012, 23:1203−1218
48. Herrnberger L, Seitz R, Kuespert S, Bösl MR, Fuchshofer R, Tamm ER: Lack of endothelial diaphragms in fenestrae and caveolae of mutant Plvap-deficient mice. Histochem Cell Biol 2012, 138: 709−724
49. Hume DA, Perry VH, Gordon S: Immunohistochemical localization of a macrophage-specific antigen in developing mouse retina: phagocytosis of dying neurons and differentiation of microglial cells to form a regular array in the plexiform layers. J Cell Biol 1983, 97: 253−257
50. Hume DA, Halpin D, Charlton H, Gordon S: The mononuclear phagocyte system of the mouse defined by immunohistochemical localization of antigen F4/80: macrophages of endocrine organs. Proc Natl Acad Sci U S A 1984, 81:4174−4177
51. Langmann T: Microglia activation in retinal degeneration. J Leukoc Biol 2007, 81:1345−1351
52. Fruttiger M: Development of the mouse retinal vasculature: angiogenesis versus vasculogenesis. Invest Ophthalmol Vis Sci 2002, 43: 522−527
53. Rousseau B, Larrieu-Lahargue F, Bikfalvi A, Javerzat S: Involvement of fibroblast growth factors in choroidal angiogenesis and retinal vascularization. Exp Eye Res 2003, 77:147−156
54. Enge M, Bjarnegård M, Gerhardt H, Gustafsson E, Kalén M, Asker N, Hammes H-P, Shani M, Fässler R, Betsholtz C: Endothelium-specific platelet-derived growth factor-B ablation mimics diabetic retinopathy. EMBO J 2002, 21:4307−4316
55. Saint-Geniez M, Maldonado AE, D'Amore PA: VEGF expression and receptor activation in the choroid during development and in the adult. Invest Ophthalmol Vis Sci 2006, 47:3135−3142
56. Kannan R, Zhang N, Sreekumar PG, Spee CK, Rodriguez A, Barron E, Hinton DR: Stimulation of apical and basolateral VEGF-A and VEGF-C secretion by oxidative stress in polarized retinal pigment epithelial cells. Mol Vis 2006, 12:1649−1659
57. Esser S, Wolburg K, Wolburg H, Breier G, Kurzchalia T, Risau W: Vascular endothelial growth factor induces endothelial fenestrations in vitro. J Cell Biol 1998, 140:947−959
58. Kamba T, Tam BYY, Hashizume H, Haskell A, Sennino B, Mancuso MR, Norberg SM, O'Brien SM, Davis RB, Gowen LC, Anderson KD, Thurston G, Joho S, Springer ML, Kuo CJ, McDonald DM: VEGF-dependent plasticity of fenestrated capillaries in the normal adult microvasculature. Am J Physiol Heart Circ Physiol 2006, 290:H560−H576
59. Oshima Y, Oshima S, Nambu H, Kachi S, Hackett SF, Melia M, Kaleko M, Connelly S, Esumi N, Zack DJ, Campochiaro PA: Increased expression of VEGF in retinal pigmented epithelial cells is not sufficient to cause choroidal neovascularization. J Cell Physiol 2004, 201:393−400
60. Schwesinger C, Yee C, Rohan RM, Joussen AM, Fernandez A, Meyer TN, Poulaki V, Ma JJ, Redmond TM, Liu S, Adamis AP, D'Amato RJ: Intrachoroidal neovascularization in transgenic mice overexpressing vascular endothelial growth factor in the retinal pigment epithelium. Am J Pathol 2001, 158:1161−1172
61. Shi X, Guo L-W, Seedial SM, Si Y, Wang B, Takayama T, Suwanabol PA, Ghosh S, DiRenzo D, Liu B, Kent KC: TGF-β/Smad3 inhibit vascular smooth muscle cell apoptosis through an autocrine signaling mechanism involving VEGF-A. Cell Death Dis 2014, 5:e1317
62. Jeon S-H, Chae B-C, Kim H-A, Seo G-Y, Seo D-W, Chun G-T, Kim N-S, Yie S-W, Byeon W-H, Eom S-H, Ha K-S, Kim Y-M, Kim P-H: Mechanisms underlying TGF-beta1-induced expression of VEGF and Flk-1 in mouse macrophages and their implications for angiogenesis. J Leukoc Biol 2007, 81:557−566
63. Nam E-H, Park S-R, Kim P-H: TGF-beta1 induces mouse dendritic cells to express VEGF and its receptor (Flt-1) under hypoxic conditions. Exp Mol Med 2010, 42:606−613
64. Park H-YL, Kim JH, Park CK: VEGF induces TGF-β1 expression and myofibroblast transformation after glaucoma surgery. Am J Pathol 2013, 182:2147−2154
65. Li Z-D, Bork JP, Krueger B, Patsenker E, Schulze-Krebs A, Hahn EG, Schuppan D: VEGF induces proliferation, migration, and TGF-beta1 expression in mouse glomerular endothelial cells via mitogen-activated protein kinase and phosphatidylinositol 3-kinase. Biochem Biophys Res Commun 2005, 334:1049−1060
66. Lee KS, Park SJ, Kim SR, Min KH, Lee KY, Choe YH, Hong SH, Lee YR, Kim JS, Hong SJ, Lee YC: Inhibition of VEGF blocks TGF-beta1 production through a PI3K/Akt signalling pathway. Eur Respir J 2008, 31:523−531

67. Walshe TE, Saint-Geniez M, Maharaj ASR, Sekiyama E, Maldonado AE, D'Amore PA: TGF-beta is required for vascular barrier function, endothelial survival and homeostasis of the adult microvasculature. PLoS One 2009, 4:e5149
68. Ma M, Ma Y, Yi X, Guo R, Zhu W, Fan X, Xu G, Frey WH, Liu X: Intranasal delivery of transforming growth factor-beta1 in mice after stroke reduces infarct volume and increases neurogenesis in the subventricular zone. BMC Neurosci 2008, 9:117
69. Park SM, Jung JS, Jang MS, Kang KS, Kang SK: Transforming growth factor-beta1 regulates the fate of cultured spinal cord-derived neural progenitor cells. Cell Prolif 2008, 41:248–264
70. Roussa E, von Bohlen und Halbach O, Krieglstein K: TGF-beta in dopamine neuron development, maintenance and neuroprotection. Adv Exp Med Biol 2009, 651:81–90
71. Zhu Y, Culmsee C, Klumpp S, Krieglstein J: Neuroprotection by transforming growth factor-beta1 involves activation of nuclear factor-kappaB through phosphatidylinositol-3-OH kinase/Akt and mitogen-activated protein kinase-extracellular-signal regulated kinase1,2 signaling pathways. Neuroscience 2004, 123:897–906
72. Carmeliet P, Ruiz de Almodovar C: VEGF ligands and receptors: implications in neurodevelopment and neurodegeneration. Cell Mol Life Sci 2013, 70:1763–1778
73. Cvetanovic M, Patel JM, Marti HH, Kini AR, Opal P: Vascular endothelial growth factor ameliorates the ataxic phenotype in a mouse model of spinocerebellar ataxia type 1. Nat Med 2011, 17: 1445–1447
74. Ma Y-Y, Li K-Y, Wang J-J, Huang Y-L, Huang Y, Sun F-Y: Vascular endothelial growth factor acutely reduces calcium influx via inhibition of the Ca2+ channels in rat hippocampal neurons. J Neurosci Res 2009, 87:393–402
75. Robinson GS, Ju M, Shih SC, Xu X, McMahon G, Caldwell RB, Smith LE: Nonvascular role for VEGF: VEGFR-1, 2 activity is critical for neural retinal development. FASEB J 2001, 15:1215–1217
76. Jin K, Zhu Y, Sun Y, Mao XO, Xie L, Greenberg DA: Vascular endothelial growth factor (VEGF) stimulates neurogenesis in vitro and in vivo. Proc Natl Acad Sci U S A 2002, 99:11946–11950
77. Kilic U, Kilic E, Järve A, Guo Z, Spudich A, Bieber K, Barzena U, Bassetti CL, Marti HH, Hermann DM: Human vascular endothelial growth factor protects axotomized retinal ganglion cells in vivo by activating ERK-1/2 and Akt pathways. J Neurosci 2006, 26: 12439–12446
78. van der Schaft TL, Mooy CM, de Bruijn WC, Bosman FT, de Jong PT: Immunohistochemical light and electron microscopy of basal laminar deposit. Graefes Arch Clin Exp Ophthalmol 1994, 232: 40–46
79. Curcio CA, Presley JB, Millican CL, Medeiros NE: Basal deposits and drusen in eyes with age-related maculopathy: evidence for solid lipid particles. Exp Eye Res 2005, 80:761–775
80. Loeffler KU, Lee WR: Is basal laminar deposit unique for age-related macular degeneration? Arch Ophthalmol 1992, 110:15–16
81. Marshall GE, Konstas AG, Reid GG, Edwards JG, Lee WR: Type IV collagen and laminin in Bruch's membrane and basal linear deposit in the human macula. Br J Ophthalmol 1992, 76:607–614
82. Xu H, Chen M, Forrester JV: Para-inflammation in the aging retina. Prog Retin Eye Res 2009, 28:348–368
83. Li F, Lan Y, Wang Y, Wang J, Yang G, Meng F, Han H, Meng A, Wang Y, Yang X: Endothelial Smad4 maintains cerebrovascular integrity by activating N-cadherin through cooperation with Notch. Dev Cell 2011, 20:291–302
84. Nguyen H-L, Lee YJ, Shin J, Lee E, Park SO, McCarty JH, Oh SP: TGF-β signaling in endothelial cells, but not neuroepithelial cells, is essential for cerebral vascular development. Lab Invest 2011, 91: 1554–1563
85. Fritsche LG, Chen W, Schu M, Yaspan BL, Yu Y, Thorleifsson G, et al; AMD Gene Consortium: Seven new loci associated with age-related macular degeneration. Nat Genet 2013, 45:433–439. 439e1–439e2
86. Yang Z, Camp NJ, Sun H, Tong Z, Gibbs D, Cameron DJ, Chen H, Zhao Y, Pearson E, Li X, Chien J, Dewan A, Harmon J, Bernstein PS, Shridhar V, Zabriskie NA, Hoh J, Howes K, Zhang K: A variant of the HTRA1 gene increases susceptibility to age-related macular degeneration. Science 2006, 314:992–993
87. Dewan A, Liu M, Hartman S, Zhang SS-M, Liu DTL, Zhao C, Tam POS, Chan WM, Lam DSC, Snyder M, Barnstable C, Pang CP, Hoh J: HTRA1 promoter polymorphism in wet age-related macular degeneration. Science 2006, 314:989–992
88. Vierkotten S, Muether PS, Fauser S: Overexpression of HTRA1 leads to ultrastructural changes in the elastic layer of Bruch's membrane via cleavage of extracellular matrix components. PLoS One 2011, 6: e22959
89. Zhang L, Lim SL, Du H, Zhang M, Kozak I, Hannum G, Wang X, Ouyang H, Hughes G, Zhao L, Zhu X, Lee C, Su Z, Zhou X, Shaw R, Geum D, Wei X, Zhu J, Ideker T, Oka C, Wang N, Yang Z, Shaw PX, Zhang K: High temperature requirement factor A1 (HTRA1) gene regulates angiogenesis through transforming growth factor-β family member growth differentiation factor 6. J Biol Chem 2012, 287:1520–1526
90. Nakayama M, Iejima D, Akahori M, Kamei J, Goto A, Iwata T: Overexpression of HtrA1 and exposure to mainstream cigarette smoke leads to choroidal neovascularization and subretinal deposits in aged mice. Invest Ophthalmol Vis Sci 2014, 55:6514–6523
91. Friedrich U, Datta S, Schubert T, Plössl K, Schneider M, Grassmann F, Fuchshofer R, Tiefenbach K-J, Längst G, Weber BHF: Synonymous variants in HTRA1 implicated in AMD susceptibility impair its capacity to regulate TGF-β signaling. Hum Mol Genet 2015, 24:6361–6373